Understanding the neural mechanisms of emotion-cognition interaction via high resolution mapping in space, time, frequency, and information transfer

Anya Dietrich[1*], Edoardo Pinzuti[1,2], Yuranny Cabral-Calderin[3], Florian Müller-Dahlhaus[4], Michael Wibral[1,5†] and Oliver Tüscher[2,4,6†]

[1*]MEG Unit, Brain Imaging Center, Goethe University, Heinrich-Hoffmann Straße 10, Frankfurt am Main, 60528, Hessen, Germany.
[2]Leibniz Institute for Resilience Research (LIR), Leibniz Institute, Wallstraße 7, Mainz, 55122, Rheinland-Pfalz, Germany.
[3]RG Neural and Environmental Rhythms, Max Planck Institute for Empirical Aesthetics, Grüneburgweg 14, Frankfurt am Main, 60322, Hessen, Germany.
[4]Department of Psychiatry and Psychotherapy, University Medical Center, Langenbeckstraße 1, Mainz, 55131, Rhineland-Palatinate, Germany.
[5]Department Data-driven Analysis of Biological Networks, Georg August University, Göttingen, Kellnerweg 6, Göttingen, 37077, Lower Saxony, Germany.
[6]Institute for Molecular Biology, Ackermannweg 4, Mainz, 55128, Rhineland-Palatinate, Germany.

*Corresponding author(s). E-mail(s): a.dietrich@med.uni-frankfurt.de;
Contributing authors: edoardo.pinzuti@lir-mainz.de; yuranny.cabral-calderin@ae.mpg.de; florian.mueller-dahlhaus@uni-mainz.de; michael.wibral@uni-goettingen.de; oliver.tuescher@lir-mainz.de;
†These authors contributed equally to this work.

Abstract

Human behaviour is inextricably linked to the interaction of emotion and cognition. For decades, emotion and cognition were perceived as separable processes, yet with mutual interactions. Recently, this differentiation has been challenged by more integrative approaches, but without addressing the exact neurophysiological basis of their interaction. Here, we aimed to uncover neurophysiological mechanisms of emotion-cognition interaction. We used an emotional Flanker task paired with EEG/FEM beamforming in a large cohort (N=121) of healthy human participants, obtaining high temporal and fMRI-equivalent spatial resolution. Spatially, emotion and cognition processing overlapped in the right inferior frontal gyrus (rIFG), specifically in *pars triangularis*. Temporally, emotion and cognition processing overlapped during the transition from emotional to cognitive processing, with a stronger interaction in β-band power leading to worse behavioral performance. Despite functionally segregated subdivisions in rIFG, frequency-specific information flowed extensively within IFG and top-down to visual areas (V2, Precuneus) – explaining the behavioral interference effect. Thus, for the first time we here show the neural mechanisms of emotion-cognition interaction in space, time, frequency and information transfer with high temporal and spatial resolution, revealing a central role for β-band activity in rIFG. Our results support the idea that rIFG plays a broad role in both inhibitory control and emotional interference inhibition as it is a site of convergence in both processes. Furthermore, our results have potential clinical implications for understanding dysfunctional emotion-cognition interaction and emotional interference inhibition in psychiatric disorders, e.g. major depression and substance use disorder, in which patients have difficulties in regulating emotions and executing inhibitory control.

Keywords: Emotion-cognition interaction, emotional interference, EEG, source reconstruction, finite element headmodel

1 Introduction

The interplay of emotional and cognitive processing is of fundamental practical importance to human behavior, and to psychopathology: emotions can drive us to excel and exceed ourselves or interfere disastrously with task performance to a degree that can change the course of our lives. Therefore, emotional interference inhibition, i.e., the inhibition of salient, distracting emotional stimuli is critical for well-being and mental health, especially as emotional stimuli receive, at least when sufficiently arousing and salient, preferred processing resources [1–3]. Hence, emotional interference inhibition requires the integration of emotional with cognitive processing in the brain by recruiting neural systems and control processes that govern both processes. Such cognitive control functions include inhibition, updating and shifting, which compete for

(limited) common processing resources [2, 4, 5]. To ensure goal-directed behavior, it is fundamental to safeguard cognitive control functioning via emotional interference inhibition against the impact of emotional interference, which can strain the common processing resources shared by cognitive and emotional processing, requiring an integration of emotion and cognition [2]. Traditionally emotion and cognition were viewed to be separate, anatomically divided processing streams, yet, recent studies revealed that they are integrated in various brain regions and modulate each other's processing [2] – acknowledging that common processing resources in the brain are limited, and multiple processes must compete for an allocation of these resources [6]. Such a competition for resources potentially causes interactions between the processes which can be beneficial or detrimental to task-performance depending on the ability for emotional interference inhibition. In general the critical information, such as emotional stimuli, may allocate resources more efficiently [3, 7], thus receiving preferred processing resources [8, 9], affecting a variety of cognitive processes. According to Pessoa's dual competition model, interactions can occur on the perceptual and executive level [2, 3] depending on the dimensionality of the emotional stimulation, such as reward or threat or task relevance. Several brain areas have been described as crucial hubs for emotion-cognition interaction and thus potentially for emotional interference inhibition, amongst them in particular, the right inferior frontal gyrus (rIFG) [10–14]. RIFG is a brain area that has been frequently linked to inhibitory control, as recently associated to response inhibition mediated by the β-band [15, 16]. This is not surprising, since many studies have shown that emotional influences on behavioral inhibition are particularly pronounced [17–19], where behavioral inhibition is a specific subtype of cognitive inhibition [20]. However, it is currently unclear if the β-band-mediated influence of the rIFG generalizes to other subtypes of cognitive inhibition, as operationalized by other paradigms. This is because previous research suggests that these subtypes are indeed separable [20] and rely on partially separate underlying neural networks [21]. Additionally, it is yet to be determined if the role of rIFG in behavioral inhibition applies only to cognitive interference or if the β-band and rIFG also mediate emotional interference and emotional interference inhibition. Commonalities between inhibitory and emotion regulation processes have been described [22]. In this study, we investigated the hypothesis that the (right) IFG is the mediator of emotional and cognitive interference as well as emotional interference inhibition. Our current understanding of the neuropsychological underpinnings of the above emotion-cognition interaction and emotional interference inhibition is limited due to the lack of studies that employ both high spatial and high temporal resolution techniques. Most studies either employ high spatial (functional magnetic resonance imaging) or high temporal (magneto/electroencephalography) resolution, but not both at the same time. Therefore, the aim of our study was to investigate the neural mechanisms of emotion-cognition interaction for the first time with combined high temporal and high spatial resolution. To this end, we employed

a large-cohort (N=121) electroencephalography (EEG) study using Finite Element Modeling of the electromagnetic forward solution and beamforming for the inverse solution. This combination allowed us to examine the interaction in space, time, frequency, and information transfer at a high temporal and high spatial resolution. The obtained understanding of the underlying neural basis of emotion-cognition interaction is particularly important as alterations in emotional and non-emotional interference processing have been observed in many patients with mental disorders, e.g., in patients with major depression [23], bipolar disorder [24], and post-traumatic stress disorder [25]. Hence, the effective integration of emotion and cognition is vital for the quality and range of many human experiences and for mental health [26].

Our study revealed that a statistical emotion-cognition interaction effect occurs during the transition from emotional to cognitive processing in the β-band in rIFG, specifically in *pars triangularis*. This neural-level interaction effect was linked to emotional interference inhibition via its correlation to the behavioral performance in the emotional Flanker task. Additionally, we found extensive frequency-specific top-down modulation from rIFG to posterior areas, which was linked to the behavioral emotional and cognitive interference effects. These findings highlight the role of the rIFG in inhibitory control, emotion-cognition interaction and emotional interference inhibition.

2 Results

2.1 Large-cohort, FEM-based EEG-beamforming for a highly resolved study of neural sources in emotion-cognition interaction

To study how emotion interferes with cognition and how this interference can be controlled, EEG data were collected from a large cohort of healthy human participants (n=121) while they performed an emotional Flanker task. During this task emotional (negative/neutral) images preceded the Flanker stimulus (incongruent/congruent). EEG data were analyzed using a combination of finite element head modeling (FEM) for the electromagnetic forward solution, and beamformer EEG source localization, yielding temporally and spatially highly resolved source data (see Fig. 1 A and Methods, Task Design section for a detailed description. See also Fig. 10 for the full analysis pipeline). We focused our analyses on the time window after onset of the Flanker stimulus, i.e., tROI Flanker in Fig. 1, because only then an emotion-cognition interaction could occur. Results from these analyses are presented in the following sections. Of note, here a main effect of emotion indicates significant differences between negative vs. neutral trials during tROI Flanker, i.e., during cognitive processing (but independent of the cognitive task condition). For analyses before Flanker stimulus onset, i.e., during the initial emotional processing following display of the emotional images only (tROI Emo), please see supplementary material section Supplementary results of source localization and Tab. A4.

2.2 Emotional interference versus emotional interference inhibition and their relation to statistical contrasts

The reader of the results presented below will have to be aware of (i) the difference between emotional interference and emotional interference inhibition, and (ii) of the differences arising from applying certain statistical contrasts (like the main effect of emotion) to behavioral data on the one hand and to neural data on the other. We speak of *emotional interference*, when emotion processing interferes with the performance in the cognitive task, i.e., when there is a *statistical main effect* of emotional valence on task performance. In the case of neural data the *statistical main effect* of emotion may reflect emotional interference as well as pure emotional processing. In contrast, we speak of *emotional interference inhibition* when there is a *statistical interaction effect* between cognitive load and emotional valence; we use the shorthand notation statistical emotion-cognition interaction in the results section, when referring to the statistical interaction.

2.3 Behavioral effects demonstrate an emotion-cognition interaction

To quantify the interference effect of emotion on goal-directed cognitive processing (emotion-cognition interaction), we used Bayesian Hierarchical linear models (for comparison with previous studies, please see additional linear mixed effect models in the Supplementary information about behavioral effects of emotion-cognition interaction and Tab. A1). In Bayesian regression models, the more plausible the experimental effects are, the more exclusively positive or negative the posterior distribution of the regression parameters are [27]. Therefore, when the 94% posterior highest density interval (HDI) contains exclusively positive or negative values we here speak of an 'effect' for brevity of the presentation, but urge the reader to inspect the full posterior distributions. In this sense, reaction time (as a measure of cognitive stimulus interference) and accuracy (as a measure of cognitive response interference) revealed effects of emotion and cognition, as well as an statistical emotion-cognition interaction effect, as all posterior HDIs distributions were negative (reaction time) or positive (accuracy). As for the emotional effect, reaction times were slower (posterior median: $\beta_E = -0.084$, posterior HDI: $[-0.097, -0.07]$) and accuracies lower (posterior median: $\beta_E = 0.19$, posterior HDI: $[0.097, 0.29]$) for negative compared to neutral trials. As for the effect of cognition, reaction times were slower (posterior median: $\beta_C = -0.91$, posterior HDI: $[-0.96, -0.86]$) and accuracies lower (posterior median: $\beta_C = 2.6$, posterior HDI: $[2.4, 2.8]$) for incongruent compared to congruent trials, corroborating well-known cognitive interference effects in the Flanker task. Overall, the behavioral effect of cognition was larger than that of emotion and the statistical emotion-cognition interaction (see Fig. 1, for detailed behavioral description see Supplementary information about behavioral effects of emotion-cognition interaction). An interaction effect of emotion and cognition was observed

for both reaction time (posterior median: $\beta_{EC} = -0.02$, posterior HDI: $[-0.035, -0.0033]$) and accuracy (posterior median: $\beta_{EC} = 0.12$, posterior HDI: $[-0.072, 0.3]$), with the effect of emotion (i.e., negative vs. neutral condition) being stronger during low compared to high cognitive load (i.e., incongruent vs. congruent condition). Thus, a stronger cognitive load might use more processing resources than a lower cognitive lead, thereby decreasing the emotional interference effect. Mixed effect model analyses showed similar results (see Supplementary information about behavioral effects of emotion-cognition interaction and Tab. A1 for comparison).

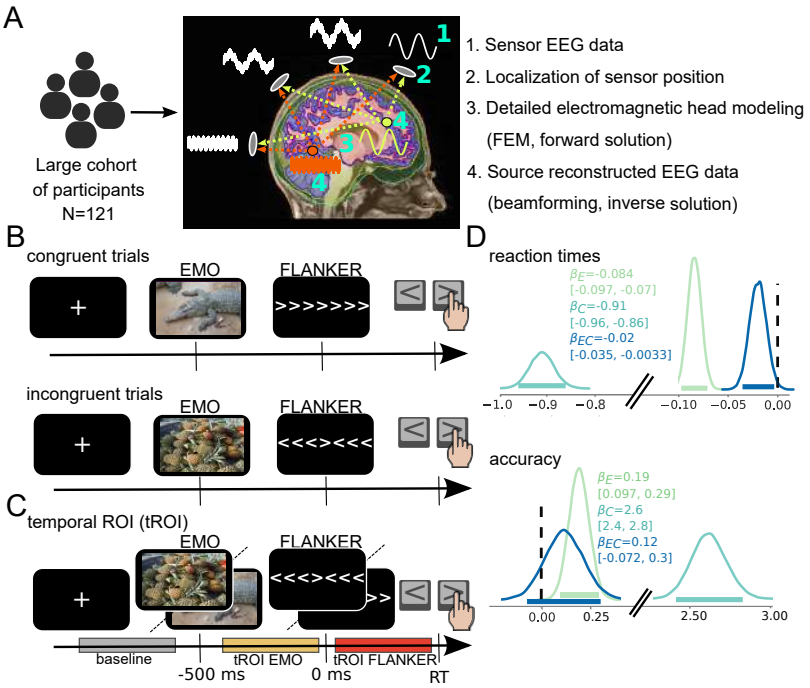

Fig. 1 Emotional Flanker task design and behavioral effects. A, We collected EEG data (1) from 121 healthy human participants and located each electrode's position (2). Using individualized Finite Element Models (FEM) of the head from structural MR images (3), we calculated electrical signal propagation in the brain (forward solution). With a beamforming algorithm, we reconstructed the signals in source space in the brain (4) – based on scalp recordings, sensor positions, and the forward solution (Please see Methods and Fig. 10). B, Basic trial design: images with neutral or negative valence (placeholder images indicate IAPS pictures) precede onset of a congruent or incongruent Flanker stimulus (time, 0 ms), determining which button to press in the subsequent behavioral response (left for a central < symbol or right for a central > symbol). C, Temporal regions of interest (tROI) of 380 ms length tROI EMO (-400 to -20 ms relative to Flanker stimulus onset, yellow) during presentation of the IAPS picture, tROI FLANKER (50 ms to 430 ms, red) after Flanker cue onset and baseline (-1000 to -620 ms relative to Flanker cue onset, gray) were used for further source reconstruction. Of note, tROIs were defined for each frequency band separately, and a duration of 380 ms is an average value; see below, Task Design and Temporal ROI definition D, Posterior distribution of the Bayesian linear regression model parameters for reaction time (cognitive stimulus interference) and accuracy (cognitive response selection interference). $\beta_{\text{meanpower}}$= β mean power, β_{C}=cognition effect, β_{E}=emotion effect and β_{EC}=interaction effect. Inset values indicate the median and 94% credible intervals of the posteriors; the latter values are also represented by horizontal bars of the same color. Priors in Tab. A3.

2.4 Source-level activity reveals rIFG as a key region for emotion-cognition interaction

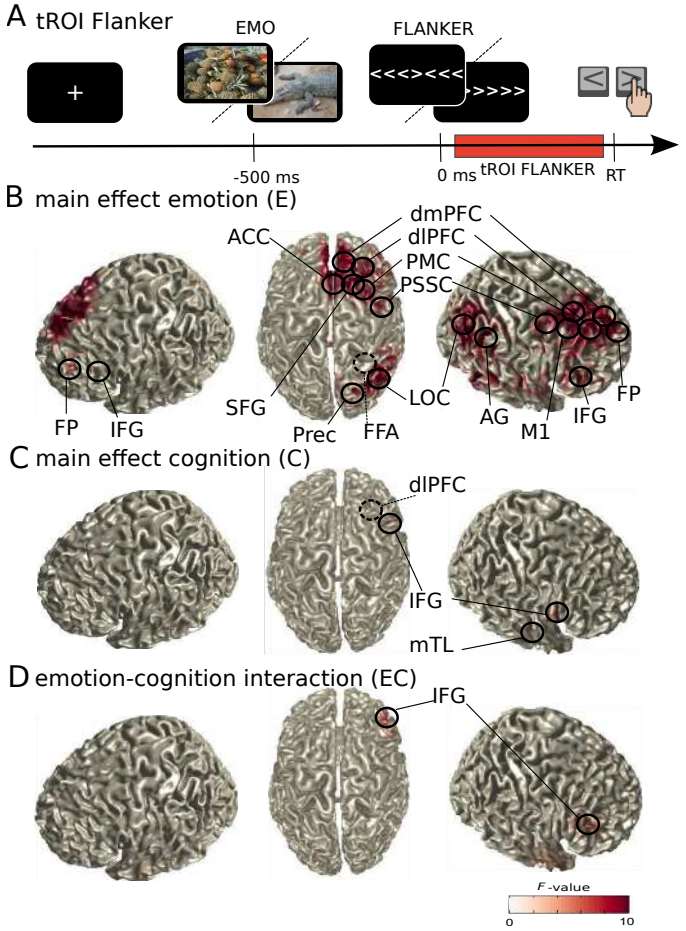

Fig. 2 Source activity in the β-band (9-33 Hz). Surface plots show significant F-values of ANOVA (cluster-based permutation test, Bonferroni corrected for four frequency bands and two time windows, alpha and clusteralpha <0.00625, n=103). Peak voxels (local extrema) of significant clusters are indicated with circles and labels (for MNI coordinates, see Tab. 1, for a detailed description of the methods, see Source analysis and Statistical analyses of source reconstruction results). Dashed circles mark peak voxels invisible in this representation. A, Task design and analyzed tROI; B, main effect of emotion (E); C, main effect of cognition (C); D, interaction effect between emotion and cognition (EC). Anatomical regions: ACC, anterior cingulate cortex; AG, angular gyrus; dlPFC, dorsolateral prefrontal cortex; dmPFC, dorsomedial prefrontal cortex; FFA, fusiform face area; FP, frontal pole; IFG, inferior frontal gyrus; LOC, lateral occipital cortex; M1, primary motor cortex; mTL, medial temporal lobe, PMC, premotor cortex; Prec, Precuneus; PSSC, primary somatosensory cortex; SFG, superior fusiform gyrus.

For analysis of neural source activity during emotion-cognition interaction, i.e., during cognitive processing after emotional image presentation (tROI Flanker), we contrasted neural source-level spectral power in a non-parametric 2×2 repeated-measures cluster permutation ANOVA with the within-subject factors emotion (negative/neutral) and cognition (incongruent/congruent). In line with our hypothesis (see Introduction, [10, 15]), rIFG was the only source significantly activated (p<1.9996e-04) by all three contrasts (n=103, main effects of emotion (*pars orbitalis*, MNI peak coordinates x=45, y=40, z=0, F-Value=10.4, p<1.9996e-04), cognition (*pars opercularis*, MNI peak coordinates x=55, y=10, z=10, F-Value= 7.9, p<1.9996e-04), and interaction effect (*pars triangularis*, MNI peak coordinates x=45, y=40, z=20, F-Value= 9.6, p<1.9996e-04)) – with these effects occurring in the β-band (Fig. 2), again, as hypothesized (see Introduction). We additionally report results from exploratory analyses in all other frequency bands during tROI Emo and tROI Flanker in the supplementary material under Supplementary results of source localization. Strikingly, peak activation locations of rIFG sources differed across contrasts: in particular, the only source showing a significant interaction effect in the β-band within the inferior frontal gyrus was the *pars triangularis*. An overview of all sources, with their respective MNI peak coordinates, can be found in Tab. 1 for the β-band and in Tab. A4 for the other frequency bands; also see (Fig. A2, A3) for θ-, (Fig. A4) for γ- (Fig. A5) and for high γ-band surface plots.

Contr.	Region (label)	Coordinat. (x,y,z)	Source F-value	point estimate (Mean)	Bootstrap 95% CI	Cluster F-value	Cluster P-value
E	Fusiform Face Area R (rFFA)	35 -50 10	16.1438	0.4319	[0.2187; 0.6455]	$5.2295e^{+0.3}$	<1.9996e-04
E	dorsomedial Prefrontal Cortex R (rdmPFC)	5 40 40	15.9367	0.4302	[0.2212; 0.6483]	5.2295e+0.3	<1.9996e-04
E	dorsolateral Prefrontal Cortex R (rdlPFC)	25 30 60	13.5796	0.3963	[0.1808; 0.6073]	5.2295e+0.3	<1.9996e-04
E	lateral Occipital Cortex R (rLOC)	35 -70 30	13.3564	0.3686	[0.1680; 0.5689]	5.2295e+0.3	<1.9996e-04
E	Frontal Pole R (rFP)	5 60 40	12.8408	0.4005	[0.1744; 0.6177]	5.2295e+0.3	<1.9996e-04
E	Angular Gyrus R (rAG)	45 -50 20	12.6571	0.3737	[0.1714; 0.5859]	5.2295e+0.3	<1.9996e-04
E	Superior Frontal Gyrus R (rSFG)	25 10 60	12.4352	0.3686	[0.1613; 0.5781]	5.2295e+0.3	<1.9996e-04
E	Premotor Cortex R (rPM)	45 0 50	11.2470	0.3553	[0.1453; 0.5647]	19.5099	<1.9996e-04
E	Inferior Frontal Gyrus R (rIFG)	45 40 0	10.4409	0.3852	[0.1510; 0.6221]	5.2295e+0.3	<1.9996e-04
E	Precuneous Cortex R (rPrec)	15 -70 50	9.7742	0.3459	[0.1311; 0.5695]	5.2295e+0.3	<1.9996e-04
E	Frontal Pole L (lFP)	-25 50 10	9.6548	0.3641	[0.1238; 0.5947]	25.9950	<1.9996e-04
E	Primary Somatosensory Cortex R (rPSSC)	45 -10 30	8.8410	0.3268	[0.1172; 0.5519]	5.2295e+0.3	<1.9996e-04
E	Inferior Frontal Gyrus L (lIFG)	-35 30 10	8.7014	0.3131	[0.1040; 0.5265]	8.7014	<1.9996e-04
E	Primary Motor Cortex R (rPrMC)	35 -20 50	8.2433	0.3131	[0.1016; 0.5327]	8.2433	<1.9996e-04
C	dorsolateral Prefrontal Cortex R (rdlPFC)	45 20 30	8.5053	0.3048	[0.1082; 0.5220]	8.5053	<1.9996e-04
C	medial Temporal Lobe R (rmTL)	65 -10 -10	8.3118	0.3278	[0.1194; 0.5716]	8.3118	<1.9996e-04
C	Inferior Frontal Gyrus R (rIFG)	55 10 10	7.9618	0.3034	[0.1010; 0.5278]	7.9618	<1.9996e-04
EC	Inferior Frontal Gyrus R (rIFG)	45 40 20	9.6267	-0.5948	[-0.9589;-0.1966]	9.6267	<1.9996e-04

Table 1 Significant β-band sources during tROI Flanker. All significant sources in the β-band are given for the contrasts (Contr.) of emotion (E), cognition (C) and statistical emotion-cognition interaction (EC). The table lists sources (Region (label)) with respective coordinates and F-values. Furthermore, it shows the point estimate in terms of source activity (mean differences of first level statistics (i.e., t-statistics) for main effects, and mean double differences for interaction effects) and the bootstrap Confidence-Interval (95% CI). Additionally, Cluster F- and P-values are reported.

2.5 Source-level activity confirms a functional parcellation of rIFG

Further inspection of the IFG sources showed that they were located in different anatomical subdivisions of the rIFG: in the anterior ventral *pars orbitalis* (IFG_{Orb}) for the main effect of emotion, in the posterior *pars opercularis* (IFG_{Op}) for the main effect of cognition, and in the anterior dorsal *pars triangularis* (IFG_{Tri}) for the interaction effect of emotion and cognition. To differentiate whether activity of these three sources originated from three separate sources or from one underlying source, we correlated activities in the virtual channels reconstructed at the peak coordinates obtained from the beamformer source reconstruction with each other. Pairwise correlations between IFG subdivisions existed ($r = 0.2844$ for IFG_{Tri} and IFG_{Op}, $r = 0.3600$ for IFG_{Tri} and IFG_{Orb}, and $r = 0.2937$ for IFG_{Orb} and IFG_{Op}), but were far from unity, suggesting separate sources and a functional segregation of emotion/cognition processing within rIFG. Notably, these three EEG sources are in correspondence with three of five rIFG clusters indicated by an fMRI meta-analysis [11] and are located within the respective clusters with striking anatomical closeness to their respective centers-of-gravity, i.e., a maximum distance below 10 mm (see Fig. 3, A). In line with the model by Hartwigsen and colleagues [11], the IFG_{Op} source, revealed by our cognition contrast, is located in a region associated to execution, compatible with an involvement in stimulus and response interference processing in our Flanker task. The IFG_{Orb} source, revealed by our emotion contrast, is located in a region associated with emotion or social processing, compatible with an involvement in emotional processing in our emotional Flanker task. Finally, the IFG_{Tri} source, revealed by our statistical emotion-cognition interaction contrast, is located in a more dorsal region associated with reasoning and adaptive control, compatible with interaction or integration of emotion and cognition in our emotional Flanker task.

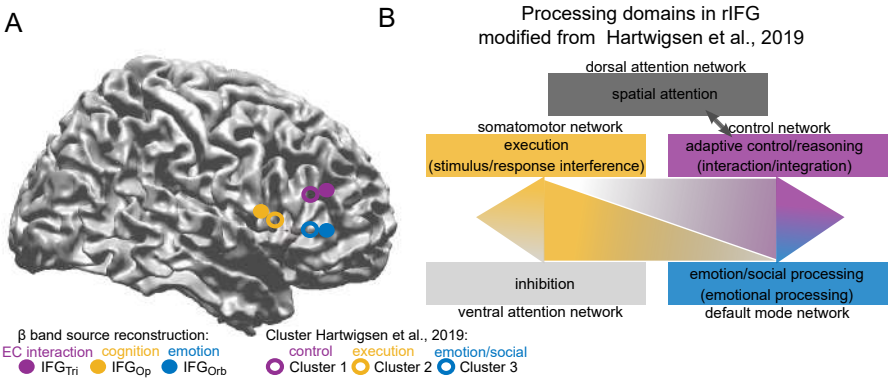

Fig. 3 Segregation of task-related β sources within rIFG. A, Three separate β sources within rIFG (IFG_{Orb}, IFG_{Op} and IFG_{Tri} represented by dots) were revealed by contrasts between task conditions (emotion: blue; cognition: yellow; statistical emotion-cognition interaction: purple), corresponding to anatomical subdivisions of IFG (*pars orbitalis*, *pars opercularis* and *pars triangularis*) and close to the centers of gravity of functional clusters (1-3, represented by circles; cluster 1: adaptive control/reasoning, purple; cluster 2: execution, yellow; cluster 3: emotion/social cognition, blue) obtained from fMRI meta analysis ([11]) B, Revision of the model by Hartwigsen and colleagues [11] indicating different processing domains in rIFG with incorporation of our findings (as indicated by brackets).

2.6 Temporal Generalization analysis reveals an emotion-cognition interaction effect in IFG pars triangularis during early cognitive processing

In order to investigate the precise temporal dynamics of emotional versus cognitive processing, and of their interaction, we performed a temporal generalization classification in each rIFG subdivision with a support vector machine (SVM) (Fig. 4) classifying the task conditions based on source-localized neural activity time courses. Thus, we were able to (1) classify between emotion (E), cognition (C), and the statistical emotion-cognition interaction (EC) processing, (2) determine the temporal unfolding of information processing in relation to these conditions, and (3) determine whether shared or isolated processing preferences exist in these rIFG subdivisions (see Fig. 3, A). This analysis revealed that information related to emotion processing can be detected long after presentation of the emotional stimulus: we received a robust classification above chance level for emotion in all three IFG subdivisions starting around 200 ms before Flanker stimulus onset and lingering until around 400 ms after Flanker stimulus presentation ($p<0.0028$, $n=103$, maximum classification accuracy and time point (Bootstrapping mean [95% CI]) was 60.1% [59.9; 60.2] at -18.5 ms [-20.8; -16.2] in IFG_{Orb}, 59.5% [59.4; 59.7] at 2.6 ms [-1.3; 6.5] in IFG_{Op} and 58.5% [55.4; 58.7] at 56.0 ms [51.8; 60.2] in IFG_{Tri}. The classification performance of the emotional process alternated between periods of high and low decoding accuracy, indicating that emotional information recurrently occupied processing resources. In contrast, accuracy of cognitive classification

after Flanker signal onset continuously increased with time up to approximately 350 ms and remained relatively high until 500 ms post Flanker stimulus onset ($p<0.0028$, $n=103$, maximum classification accuracy and time point (Bootstrapping mean[95% CI]) was 64.9% [64.7; 65.1] at 354.1 ms [351.1; 357.1] in IFG_{Orb}, 65.3% [65.1; 65.5] at 365.4 ms [362.5; 368.2] IFG_{Op} and 65.0% [64.8; 65.2] at 339.0 ms [189.8; 286.0] in IFG_{Tri}, indicating that resources devoted to this process ramp up over time. As expected, cognitive processes could reliably be classified above chance level after onset of the Flanker stimulus in all three subdivisions. Importantly, at the moment when cognitive information processing entered the network, i.e., when the SVM first classified the cognitive task conditions correctly, the strongest, temporally specific, statistical interaction effect between emotion and cognition took place in IFG_{Tri} ($p<0.0028$, $n=103$, maximum classification accuracy (mean, [95% Bootstrap-CI]) was 55.8% [55.3; 55.9] at 216.8 ms [214.5; 219.0] in IFG_{Tri}. Of note, the strongest interaction effect thus did not occur when the decodability of both processes was highest, but rather when the cognitive process entered the emotionally loaded network, presumably introducing a competition over processing resources. Together with our beamforming results, these findings strongly imply that IFG_{Tri} serves as the critical subdivision for emotion-cognition interaction.

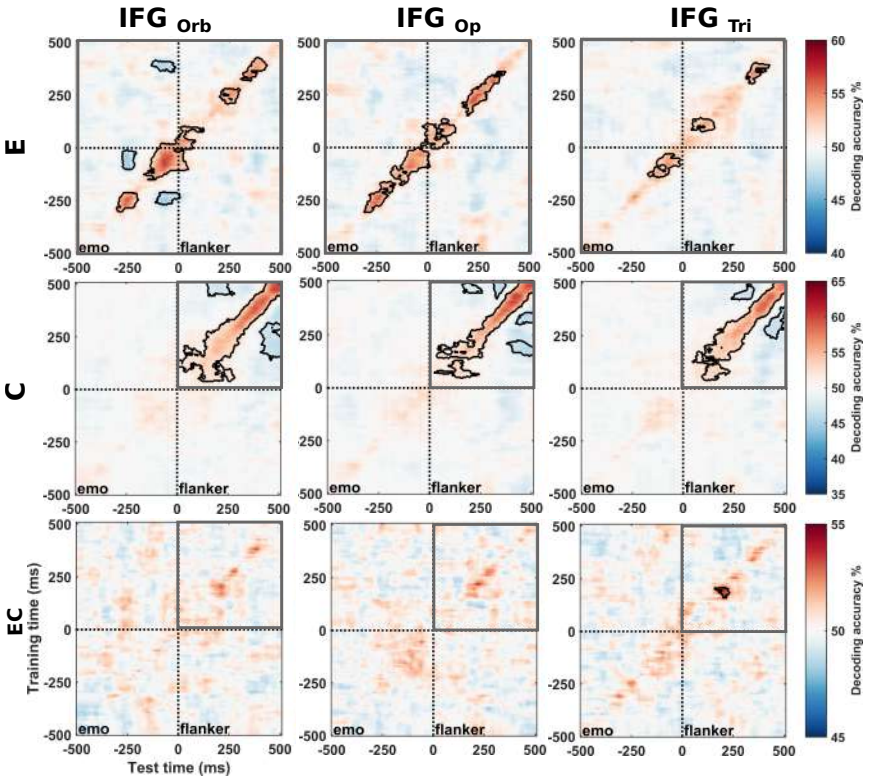

Fig. 4 Temporal Generalization of task condition classification. Temporal generalization matrices for the three contrasts emotion (E), cognition (C) and their interaction (EC) (rows) in the three IFG subdivisions IFG_{Orb} (emotion), IFG_{Op} (cognition) and IFG_{Tri} (EC interaction) (columns). In each panel, a classifier was trained for each time sample (vertical axis: training time) and tested on all other time samples (horizontal axis: testing time), for each subject separately. The resulting individual decoding matrices were averaged across subjects, decoding contrasts and IFG subdivisions. Black contours indicate significant decoding values. Statistical tests used a cluster-size permutation procedure using a cluster defining threshold of $p < 0.0028$, and a corrected significance level of $p < 0.0028$ ($n = 103$). Grey boxes indicate time window of statistical test: contrast E was computed over the full time-range (-0.5-0.5 ms); since effects of contrasts C or EC can logically be present only after Flanker stimulus onset, a restricted time-range of 0-0.5 ms was used for these contrasts. Dotted lines indicate Flanker stimulus onset (0 (ms),"Flanker").

2.7 β-band emotion-cognition interaction in IFG pars triangularis is behaviorally relevant

Given the findings described above (see section: Source-level activity reveals rIFG as a key region for emotion-cognition interaction), we sought to determine the behavioral relevance of β activity in IFG_{Tri} for emotion-cognition interaction. Since interactions can be of both signs (i.e., negative and positive), we calculated the interaction effect ((negative incongruent − neutral incongruent) − (negative congruent − neutral congruent)) in the β-band (9 − 33

Hz, $0.05 - 0.43$ s) and searched for the minimum and maximum β power interaction values for each individual subject, respectively, as we were specifically interested in individual effects of emotion-cognition interaction. We then correlated the individual maximum and minimum β interaction power values (i.e. the double differences described above) and the individual mean reaction time (stimulus interference) and mean response accuracy (response interference) (Fig. 5, A). In an analysis of Bayes factors, there was extreme evidence for a correlation of response accuracy and the maximum (BF_{10}=984e+03; posterior median: $\beta = -0.513$, posterior HDI: $[-0.646, -0.362]$) and minimum (BF_{10}= 694; posterior median: $\beta = 0.391$, posterior HDI: $[0.220, 0.545]$) β interaction power. For reaction time, there was moderate evidence for a correlation with the maximum β interaction power (BF_{10}= 9.368; posterior median: $\beta = 0.282$, posterior HDI: $[0.099, 0.452]$), but no evidence for a correlation with minimum β interaction power (BF_{10}=0.272; posterior median: $\beta = -0.123$, posterior HDI: $[-0.308, 0.069]$) (see Fig. 5, B). Together, these findings suggest that the stronger the β-band interaction is, the worse is the behavioral performance. Thus, stronger β-band emotion-cognition interaction means less emotional interference inhibition, means more emotional and cognitive interference as visible in overall worse behavioral performance.

In order to understand whether only β-band power in relation to the statistical emotion-cognition interaction is informative for the behavioral outcome, or whether also β-band power in general (average power), or β-band effects in relation to emotion or cognition, were behaviorally relevant, we employed an additional Bayesian linear regression analyses including each β-power measure as a factor in the model (see Fig. 5, C). As expected given the correlation results, the parameters for the β power interaction values were by far the most influential as shown by the model posteriors: The posterior distributions of the regression parameters for predicting the reaction time based on the maximum cluster were: posterior median: $\beta_{\text{meanpower}} = 0.056$, posterior HDI: $[-0.15, 0.25]$; posterior median: $\beta_E = -0.16$, posterior HDI: $[-0.3, -0.012]$; posterior median: $\beta_C = 0.14$, posterior HDI: $[-0.026, 0.3]$; posterior median: $\beta_{EC} = 0.32$, posterior HDI: $[0.089, 0.56]$. The posterior distributions for predicting the accuracy based on the minimum cluster were: posterior median: $\beta_{meanpower} = 0.2$, posterior HDI: $[0.003, 0.4]$; posterior median: $\beta_E = -0.034$, posterior HDI: $[-0.17, 0.097]$; posterior median: $\beta_C = -0.04$, posterior HDI: $[-0.18, 0.1]$; posterior median: $\beta_{EC} = 0.5$, posterior HDI: $[0.26, 0.74]$, and based on the maximum cluster: posterior median: $\beta_{meanpower} = 0.036$, posterior HDI: $[-0.15, 0.21]$; posterior median: $\beta_E = 0.098$, posterior HDI: $[-0.034, 0.23]$; posterior median: $\beta_C = 0.075$, posterior HDI: $[-0.07, 0.22]$; posterior median: $\beta_{EC} = -0.69$, posterior HDI: $[-0.9, -0.47]$. The posteriors for predicting the mean reaction time based on the minimum cluster were posterior median: $\beta_{meanpower} = -0.085$, posterior HDI: $[-0.31, 0.12]$; posterior median: $\beta_E = 0.072$, posterior HDI: $[-0.07, 0.22]$; posterior median $\beta_C = -0.059$, posterior HDI: $[-0.21, 0.093]$; posterior median: $\beta_{EC} = -0.14$, posterior HDI: $[-0.4, 0.11]$). In line with our correlation results (Fig. 5, B) these findings

indicate that, indeed, specifically the statistical emotion-cognition interaction in the β-band is the key factor for determining the behavioral outcome of emotional and cognitive interference and of its inhibition, rather than overall β-band power or β-band power effects from sources located with respect to the main effects of emotion or cognition only.

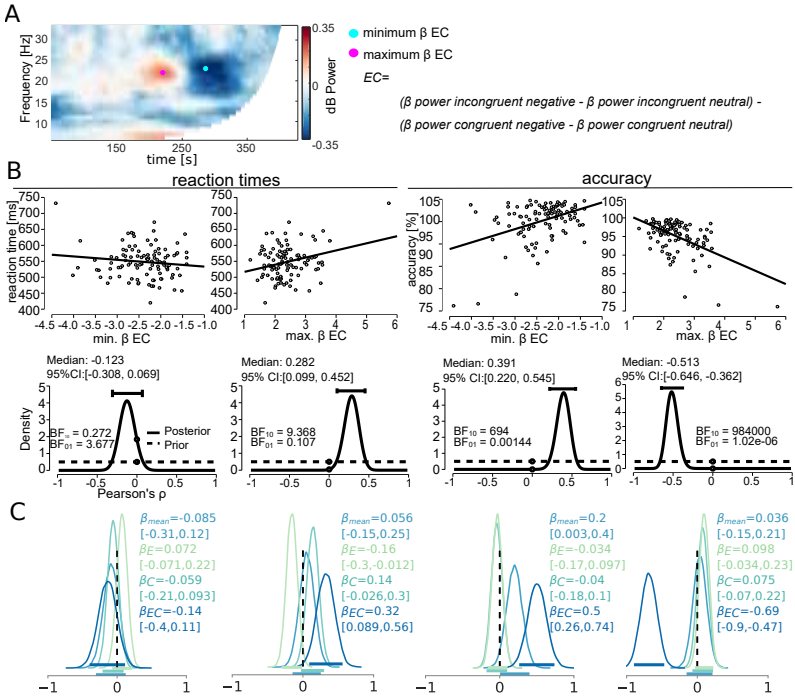

Fig. 5 Behavioral prediction based on maximum and minimum β power interaction values. A, Time-Frequency Representation for the statistical emotion-cognition interaction contrast in an exemplary subject with maximum (magenta dot) and minimum (cyan dot) β power interaction values during tROI Flanker. Overall, the averaged individual maximum β interaction frequency was 20.93 Hz and appeared 237 ms after Flanker stimulus onset, whereas the averaged individual minimum β interaction frequency was 20.71 Hz and appeared 248 ms after Flanker stimulus onset. B, Bayesian correlation of β power interaction values (maximum and minimum) with mean reaction time and response accuracy (per subject, n=103). Correlation coefficients ρ are shown with prior (dashed line) and posterior distributions (solid line), median, central 94% credible interval, and Bayes Factors BF10 and BF01. Regression plots are shown above each distribution. C, Posterior distributions of the regression coefficients of the Bayesian linear regression models predicting mean reaction times and accuracy (per subject, n=103) with median and 94% credible interval (horizontal bars) for β_{mean}= β mean power, β_{C}=cognition effect, β_{E}=emotion effect and β_{EC}=interaction effect of maximum and minimum β power values. Graphs follow the same order as in panel B and show (from left to right) the posterior distributions of models predicting mean reaction times based on minimum β power values, predicting mean reaction times based on maximum β power values, predicting mean accuracy based on minimum β power values, predicting accuracy based on maximum β power values. See Bayesian correlation of min/max β power interaction values with behavioral measures and Bayesian linear regression of β power with behavioral measures for a detailed description of the methods.

2.8 Integration and segregation of emotional and cognitive information within IFG

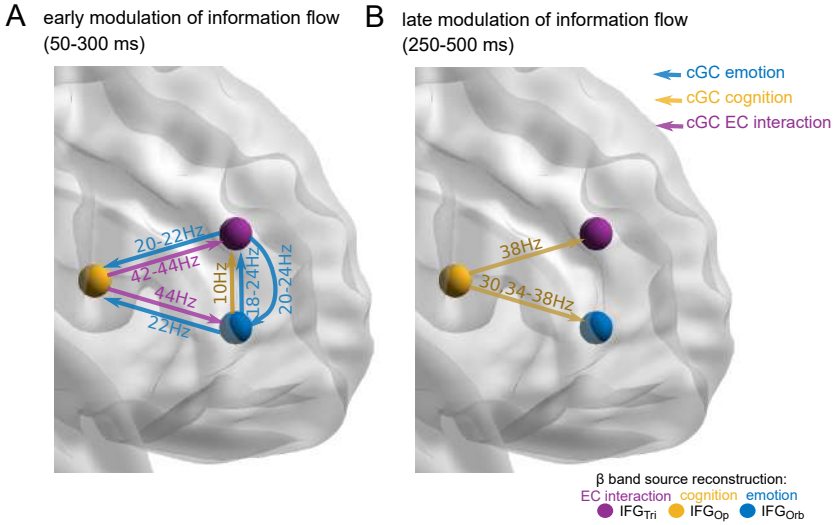

Fig. 6 Spectrally-resolved conditional Granger Causality (cGC) within IFG subdivisions. Blue (IFG_{Orb}, emotion (E)), yellow (IFG_{Op}, cognition (C)), and purple (IFG_{Tri}, statistical emotion-cognition interaction (EC)) nodes refer to the IFG sources in the β-band (see Fig. 2 and Fig. 3). Arrows indicate a significant spectral-cGC modulation (information flow) related to main effects of emotion (E, blue) and cognition (C, yellow) and their interaction (EC, purple) (see Methods), respectively. A cluster-based permutation ANOVA was used to identify significant differences between E, C, and EC contrasts. Significant differences after Bonferroni correction ($n = 103$ for all links, six links and two windows tested, $\alpha_{crit} = 0.05/12$) are reported with their significant spectral range. A, spectral cGC at early processing, 50-300 ms after Flanker stimulus onset. The modulation of information flowing between IFG nodes is mostly related to emotion and the statistical emotion-cognition interaction (blue and purple arrows). B, spectral cGC in the later time window 250-500 ms after Flanker stimulus onset. The modulation of information flow is mostly related to cognition (yellow arrow). Statistics were computed for n=103. For an overview of significant participants, links, and frequencies, please see Tab. 2.

Given the functional segregation of IFG subdivisions (see Source-level activity reveals rIFG as a key region for emotion-cognition interaction, Source-level activity confirms a functional parcellation of rIFG [11]) and the specific and behaviorally relevant role of IFG_{Tri} for emotion-cognition interaction, as well as the known anatomical interconnectivity of IFG subdivisions [28], we next aimed to understand the exact temporal and spectral dynamics of information flow within rIFG. To this end, we computed spectrally-resolved conditional Granger Causality (cGC) in two time windows (i.e., an early processing (visual to cognitive) phase [50-300 ms] and a late processing (cognitive to

motor) phase [250-500 ms]) after Flanker stimulus onset between the three IFG subdivisions obtained from our source reconstruction contrasts cognition (IFG_{Op}), emotion (IFG_{Orb}) and statistical emotion-cognition interaction (IFG_{Tri})(see Non-parametric Granger Causality Analysis and Statistical testing of cGC for detailed description). Results showed significant spectral-cGC differences between IFG subdivisions, with the early time window (50-300 ms) primarily showing main effects of emotion in the β frequency (18-24 Hz, $p < 9.99e-05$, $n = 103$, see also Tab. 2 for an overview), indicating lingering emotional processing. During this time window, IFG_{Orb} and IFG_{Tri} acted as both senders and receivers of emotional information, while IFG_{Op} only served as a receiver. In contrast, cognitive information was only sent from IFG_{Orb} to IFG_{Tri}, at a frequency of 10 Hz ($p < 9.99e-05$, $n = 103$) (Fig. 6, Tab. 2).

Contrast	toi	Hz	Link	N(sig.)	p-values	p.e. (Mean)	Bootstrap 95% CI
E	early	22-22 Hz	$IFG_{Orb} \longrightarrow IFG_{Op}$	103	9.999e-0.5	0.0059	[0.0022; 0.0098]
E	early	18-24 Hz	$IFG_{Orb} \longrightarrow IFG_{Tri}$	103	9.999e-0.5	-8.8583e-04	[-0.0049; 0.0029]
E	early	20-22 Hz	$IFG_{Tri} \longrightarrow IFG_{Op}$	103	9.999e-0.5	0.0072	[0.0033; 0.0118]
E	early	20-24 Hz	$IFG_{Tri} \longrightarrow IFG_{Orb}$	103	9.999e-0.5	0.0083	[0.0041; 0.0125]
C	early	10-10 Hz	$IFG_{Orb} \longrightarrow IFG_{Tri}$	103	9.999e-0.5	-0.0077	[-0.0127; -0.0025]
EC	early	42-44 Hz	$IFG_{Op} \longrightarrow IFG_{Tri}$	103	9.999e-0.5	0.0135	[0.0075; 0.0229]
EC	early	44-44 Hz	$IFG_{Op} \longrightarrow IFG_{Orb}$	103	9.999e-0.5	0.0118	[0.0061; 0.0204]
C	late	30-30 Hz	$IFG_{Op} \longrightarrow IFG_{Orb}$	103	9.999e-0.5	-0.0044	[-0.0076; -0.0017]
C	late	34-38 Hz	$IFG_{Op} \longrightarrow IFG_{Orb}$	103	9.999e-0.5	-0.0051	[-0.0083; -0.0025]
C	late	38-42 Hz	$IFG_{Op} \longrightarrow IFG_{Tri}$	103	9.999e-0.5	-0.0053	[-0.0088; -0.0026]

Table 2 Overview of significant links within IFG. Table shows in which contrast, temporal region of interests (toi), frequencies (Hz) a link was significant in for how many participants (N(sig.)) with respective p-values of frequency-resolved group-level statistics. Point estimates (mean) and 95% confidence intervals from bootstrapping are reported. The frequency-agnostic individual level statistic was done for n=103; all reported links reached the lowest possible p-value in the permutation test. Threshold for significance was $p < 0.0042$. See Fig. 6

While receiving emotional information in the β frequency band, IFG_{Op} sent information related to statistical emotion-cognition interaction to both other subdivisions, at a frequency in the low γ range (42-44 Hz$p < 9.99e-05$, $n = 103$). Thus, emotion-cognition interaction seems to take place when the network is loaded with emotional processing, but before cognitive processing is firmly established. This finding is fully in line with findings from our temporal generalization analysis (Fig. 4). During the late time window (250-500 ms) a shift in processing style within the IFG from emotional to cognitive processing occurred, with cognitive information flowing primarily from IFG_{Op} to both other IFG subdivisions in the high β/low γ frequency range (30 to 38 Hz, $p < 9.99e-05$, $n = 103$). Of note, these frequency ranges are similar to the ones reported by Schaum and colleagues [15] in relation to a purely cognitive response inhibition task. In summary, while information related to emotional processing, and emotion-cognition interaction, is distributed during an early processing phase after Flanker stimulus onset in the IFG network, information related to cognitive processing is mainly sent by IFG_{Op} during a later

phase. In addition, data clearly support functional integration of information in a temporal and frequency-specific manner in the IFG network concurrent with functional segregation of anatomical IFG subdivisions, as described above (Temporal Generalization of condition classification).

2.9 Top-down long-range inter-regional modulation by IFG

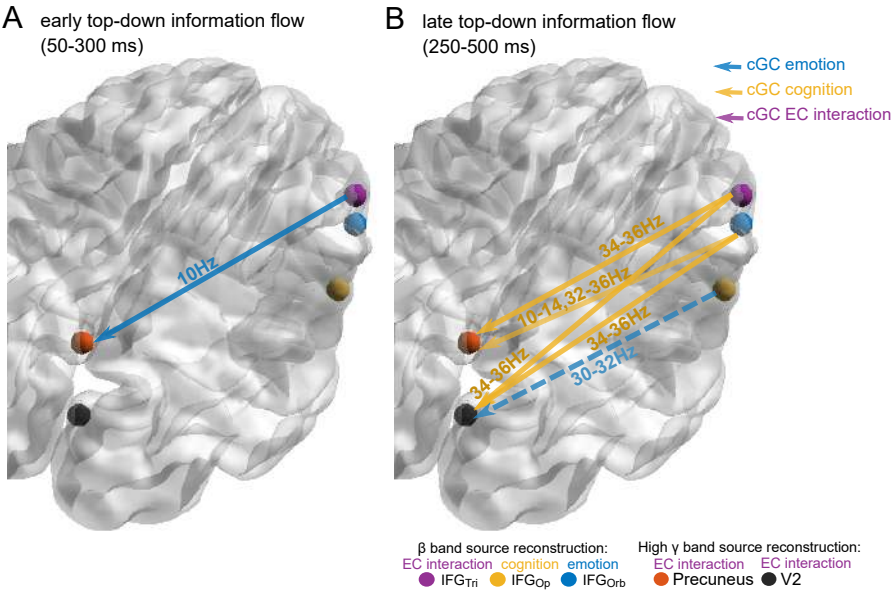

Fig. 7 Spectrally-resolved conditional Granger Causality (cGC) between IFG subdivisions and Precuneus and V2. Blue, yellow and purple nodes refer to the IFG subdivisions reconstructed in the β-band (see Fig. 2 , Fig. 3 and Fig. 6); orange and black nodes refer to Precuneus and V2, reconstructed in the high γ band (see supplemental material). Blue, yellow and purple arrows indicate a significant spectral cGC modulation in emotion (E), cognition (C) and statistical emotion-cognition interaction (EC), respectively (see Methods for the definitions of these contrasts). Significant differences after Bonferroni correction (i.e., six links and two windows tested, $p<0.0042$) are reported as solid arrows with corresponding contrasts and significant spectral ranges. Close to significant links ($p<0.00559$) are denoted as dashed arrows. A, Spectral cGC at 50-300 ms after Flanker stimulus onset, showing IFG_{Tri}-Precuneus modulation related to emotional processing. B, Spectral cGC at 250-500 ms relative to Flanker stimulus onset, showing IFG_{Tri} and IFG_{Orb} modulation of Precuneus and V2 related to cognitive processing. The frequency-agnostic individual level statistic was done for n=103. The frequency-resolved group-level statistics was done on significant participants, links, and frequencies, please see Tab. 2.

Beyond the behavioral significance of IFG in emotion-cognition interaction, we next sought to understand whether IFG exerts top-down control [29] over other areas relevant for emotion-cognition interaction with known anatomical connections to IFG [28]. As rIFG was the only source exhibiting a statistical

emotion-cognition interaction effect in the β-band (see Fig. 2), we had to search for potential target sources of top-down control in other frequency bands. In the high-γ band we indeed identified two posterior sources, i.e., Precuneus (Fig.A5, n=103, MNI peak coordinates =-5, y=-60, z=30, F-Value=7.8551, p<1.9996e-04) and visual area V2 (n=103, MNI peak coordinates =5, y=-80, z=20, F-Value=7.9948, p<1.9996e-04), that showed a statistical emotion-cognition interaction effect (see Supplementary results of source localization). Next, we thus conducted a spectrally-resolved cGC analysis including all three IFG subdivisions (IFG_{Orb}, IFG_{Op}, and IFG_{Tri}) and both posterior sources (Precuneus and V2) (Fig. 7) to reveal potential top-down modulations (see Non-parametric Granger Causality Analysis and Statistical testing of cGC for detailed description of cGC analysis). In the early time window [50-300ms] we found significant emotion effects on information flow (p<0.0042, Bonferroni corrected for time windows and links; details in Table 3) from IFG_{Tri} to Precuneus at 10 Hz ($p = 0.00369$, $n = 97$). In the later time window [250-500 ms] we found significant cognitive effects on information flow from IFG_{Tri} to Precuneus and V2 at 34-36 Hz ($p = 0.00439$, $n = 97$), and from IFG_{Orb} to Precuneus at 10-14 ($p = 0.00309$, $n = 97$) and 32-36 Hz ($p = 0.00119$, $n = 97$) and to V2 at 34-36 Hz ($p = 0.00349$, $n = 85$). Further, we found a close to significant emotion effect on information flow from IFG_{Op} to V2 at 30-32 Hz ($p = 0.00559$, $n = 100$). No significant interaction effect of emotion and cognition on information flow was found in the top-down direction from IFG to the posterior areas. However, we again observed a switch in processing style, as cGC from IFG_{Tri} signals emotional information in the early phase of processing, while in the later phase cGC from IFG_{Orb} signals cognitive information. These findings highlight a temporally-, spectrally- and context-specific long-range modulation from rIFG to Precuneus and V2.

Contr.	toi	Hz	Link	N	p-values	p.e. (Mean)	Bootstrap 95% CI
E	early	10-10 Hz	$IFG_{Tri} \longrightarrow$ Prec	97	0.00396	-0.0019	[-0.0035; -4.2407e-04]
E	late	30-32 Hz	$IFG_{Op} \longrightarrow$ V2	100	0.00559	-0.0014	[-0.0024; -3.9837e-04]
C	late	34-36 Hz	$IFG_{Tri} \longrightarrow$ Prec	97	0.00439	-0.0012	[-0.0022; -2.7789e-04]
C	late	34-36 Hz	$IFG_{Tri} \longrightarrow$V2	91	0.00409	-0.0012	[-0.0021; -3.8342e-04]
C	late	34-36 Hz	$IFG_{Orb} \longrightarrow$ V2	85	0.00349	-0.0014	[-0.0023; -4.2687e-04]
C	late	10-14 Hz	$IFG_{Orb} \longrightarrow$ Prec	97	0.00309	0.0020	[3.4456e-04; 0.0038]
C	late	32-36 Hz	$IFG_{Orb} \longrightarrow$ Prec	97	0.00119	-0.0014	[-0.0026; -4.4325e-04]

Table 3 Overview of significant top-down links from IFG to Prec and V2. Table shows in which contrast (Contr.), temporal region of interests (toi), frequencies (Hz) the link was significant in how many participants (N) with respective p-values of frequency-resolved group-level statistics. Point estimates (mean) and 95% confidence intervals from bootstrapping are reported. The frequency-agnostic individual level statistic was done for n=103. Threshold for significance was $p < 0.0042$. See Fig. 7.

2.10 The Top-down Influence from IFG to Precuneus and V2 explains the behavioral interference effect

Finally, we studied the behavioral relevance of the long-range inter-regional modulation by rIFG. To this end, we determined which of the above identified links are relevant for the behavioral performance by correlating changes in spectral cGC on these links with the behavioral measures of the interference effects in our emotional Flanker task, i.e., reaction time (stimulus interference inhibition) and response accuracy (response interference inhibition) as well as the respective emotional interference effects (see Correlation of top-down Granger Causality with behavior). We found that the change in information flow from IFG_{Orb} to Precuneus and V2, and from IFG_{Op} to V2 predicted behavior: for cognition, the change in cGC from IFG_{Orb} to V2 (34-36Hz connection; posterior median: $\beta = -0.22$, posterior HDI: $[-0.45, -0.0074]$) was negatively correlated with the change in reaction time and the same held for the information flow Precuneus (32-36 Hz connection; posterior median: $\beta = 0.22$, posterior HDI: $[-0.1, 0.44]$). For emotion, the change in cGC from IFG_{Op} to V2 (30-32 Hz connection) was positively correlated with reaction time (posterior median:$\beta = 0.17$, posterior HDI: $[0.068, 0.26]$) and negatively correlated with response accuracy (posterior median:$\beta = -0.24$, posterior HDI: $[-0.34, -0.15]$) (see Fig 8,A). The other links were not informative for predicting the behavior. Additionally, we computed Bayesian linear models to predict the interference effects (Δ RT or Δ acc) caused by emotion and cognition, respectively, on behavioral performance, based on a model including all links originating in one subdivision as factors. That is, the cognitive information flow from IFG_{Orb} to both Precuneus and to V2 were used as factors in the same model to predict Δ reaction time (incongruent | congruent). Fig. 8,B shows that the difference in top-down modulation (incongruent − congruent) from IFG_{Orb} to Precuneus was negatively associated with the cognitive interference effect on reaction time (posterior median:$\beta = -0.27$, posterior HDI: $[-0.55, -0.0021]$), i.e., the stronger the difference in cognitive information flow was, the less impaired was the participants' behavior due to the incongruent Flanker stimulus (i.e., cognitive interference). No association was seen for the cognitive information from IFG_{Orb} to V2 (posterior median:$\beta = -0.035$, posterior HDI: $[-0.3, 0.25]$). In contrast, the difference in emotional top-down modulation (negative − neutral) from IFG_{Op} to V2 was associated to the emotional interference effect on reaction time (negative − neutral) (posterior median: $\beta = 0.12$, posterior HDI: $= [-0.065, 0.3]$) and accuracy (posterior median: $\beta = -0.14$, posterior HDI: $[-0.32, 0.046]$), i.e., the stronger the emotional information flow from IFG_{Op} to V2 in the negative condition was, the worse the behavioral performance was in the negative compared to the neutral conditions for both stimulus and response interference. Hence, top-down effects on emotional processing negatively impacted goal-directed, task-relevant behavior in our task, while those on cognitive processing improved it.

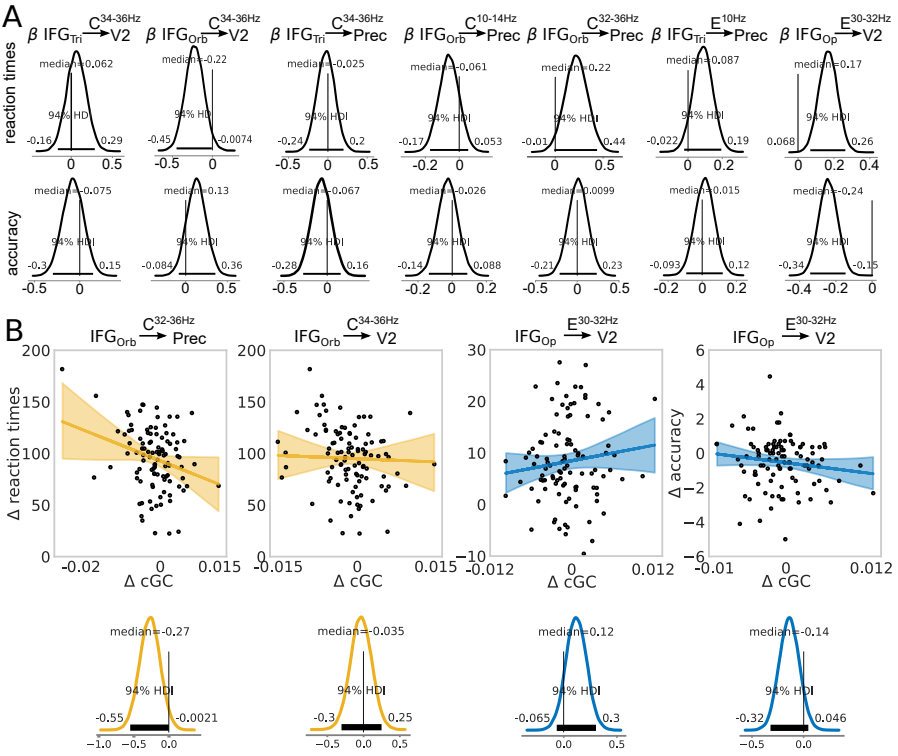

Fig. 8 Spectrally-resolved cGC from IFG to Precuneus and V2 correlates with behavior. A, Posterior distributions of the Bayesian linear regression model parameters for models with cGC links from IFG subdivisions to Precuneus (Prec) or visual area V2 (see black arrow above posterior) as predictors, and behavioral measures (reaction time and accuracy) as outcomes. Contrast and frequency information can be found above the black arrows. Inset values indicate the median and 94% credible intervals of the posteriors; the latter values are also represented by the horizontal bars in black. Links with a 94% credible interval that were entirely positive or negative were used for subsequent Bayesian multiple linear regression models. B. Linear regression for a regression of the differences between conditions (E, C) in behavior (reaction times, accuracies) on the differences between conditions for cGC (ΔcGC), for cGC from IFG_{Orb} to Prec and V2, and IFG_{Op} to V2, respectively. Corresponding marginal posterior distributions are shown below. See Correlation of top-down Granger Causality with behavior for a detailed description

3 Discussion

This high-powered EEG study uncovered neurophysiological mechanisms of emotion-cognition interaction, providing evidence for an overlap and interaction between emotion and cognition processing in rIFG. Information related to emotion, cognition, and their interaction flowed between different subdivisions of rIFG in a frequency-specific manner. A statistical interaction of the factors emotion and cognition, indicating emotional interference inhibition, was specifically confined to a modulation in *pars triangularis* of rIFG in the β-band activity during the transition from emotional to cognitive processing,

which was linked to performance in our emotional Flanker task. Moreover, rIFG exerted long-range top-down modulation of visual areas, which predicted the behavioral interference effects. Findings corroborate the notion that information related to emotion, cognition, and their interaction both segregates and integrates functionally and temporally in rIFG, the activity of which modulates top-down posterior, perceptive areas of the brain to shape behavioral performance.

Our study found that emotion and cognition-related neural activity interact in a single frontal cortical area, the rIFG, indicating that this brain area serves as a crucial hub for controlling emotional interference of cognitive processing, i.e., emotional interference inhibition. This concurs to fMRI findings [2, 3] that the IFG is affected by emotional processing, and that it is a specific site of convergence and integration of emotional and cognitive processing [2, 10], contributing to the control of behavior [30]. It also clearly argues against the traditional view that emotion and cognition originate from separate processing streams (see [31] for a push-pull relationship model). We precisely determined one subdivision of the rIFG, specifically the *pars triangularis*, as the site most important for emotion-cognition interaction. Emotional processing resides more in *pars orbitalis* and cognitive processing more in *pars opercularis*. Hence, we show a functional and anatomical segregation within the rIFG. The very same functional and anatomical segregation of rIFG at almost identical anatomical locations can be found in meta-analytic fMRI evidence by [11]. Our findings also add to a previous report of parallel but distinct processing streams originating from ventral and dorsal rIFG, respectively, in the context of response inhibition [32], and are in line with the notion of posterior to anterior and dorsal to ventral gradients in the frontal cortex, as observed for the insula [33] and the inferior frontal gyrus [11].

Our findings go beyond this previous evidence in providing a deeper understanding of the temporal and spectral dynamics of emotion-cognition interaction. The temporal resolution of fMRI – which is in the order of 500 ms – is clearly insufficient to demonstrate a true emotion-cognition interaction at the timescale of neural activity, which changes in the order of tens of milliseconds. Therefore, we employed state-of-the-art finite element head modeling-based EEG-beamforming in a large cohort of subjects and conservative statistics in order to achieve a spatio-temporal resolution that is clearly sufficient to demonstrate true interactions at the neural level.

Analysis of the temporal dynamics (temporal generalization by SVM) revealed lasting emotional processing in all subdivisions of rIFG long into the phase of cognitive processing, while cognitive processing increased with time after the onset of the cognitive task (i.e., Flanker stimulus onset, see Fig. 4). Hence, we observed two parallel, rather than two consecutive, processes competing for the same processing resources. Competition for limited neural resources thus necessitates an interaction of both processes on the neural and process level, which is dominantly handled in *pars triangularis* of rIFG as indicated

by the statistical interaction effect (Fig. 2 and Fig. 9). The above competition for neural resources follows more general theories of limited (neural and cognitive) resources [2], stating that present emotional stimuli demand processing resources. As soon as a cognitive task appears, the cognitive process competes for such resources in order to respond correctly to the task at hand. Our highly resolved temporal data offer a mechanism of how this competition unfolds over time: the interaction specifically occurs temporally focused when the entering cognitive processing forces a redistribution of processing resources. Based on these findings, we propose a process model in which the use of neural resources of one process overrides those of the other in rIFG during the competition of emotional and cognitive processing demands (see Fig. 9), highlighting the role of *pars triangularis* in this context. Interestingly, significant emotional processing seems to start over 100 ms later in *pars triangularis* compared to *pars orbitalis* and *pars opercularis* (see Fig. 4), further corroborating the notion that *pars triangularis* may have a supervisory role among the three rIFG subdivisions.

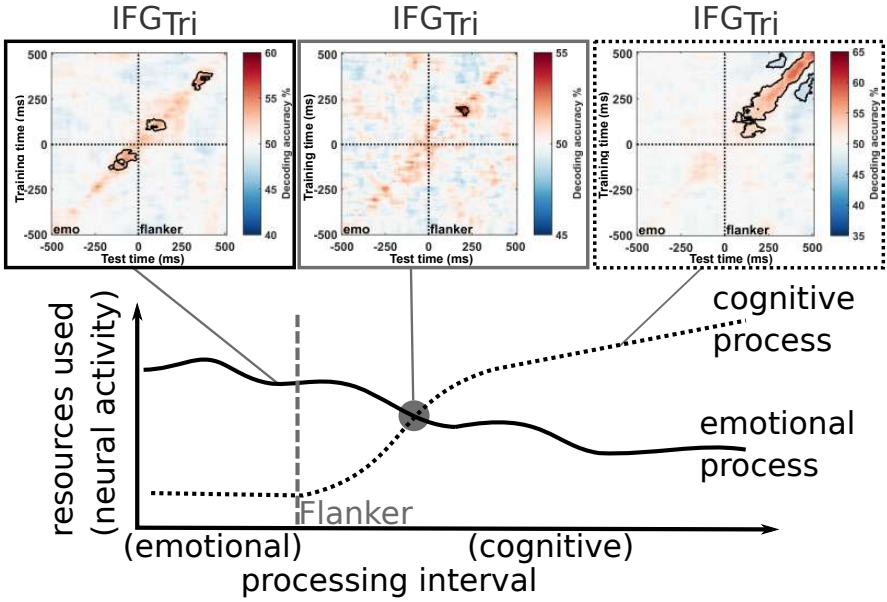

Fig. 9 Neurophysiological model of emotion-cognition interaction. Emotional and cognitive processing compete for limited resources, with resources allocated to emotional processing decreasing during the ramp-up of cognitive processing. Emotion-cognition interaction occurs in $rIFG_{tri}$ at the cross-over of resource allocation to emotional and cognitive processing (also compare Fig. 4).

Emotion-cognition interaction in the rIFG was mediated by β-band activity. This is consistent with previous research suggesting that β-band plays a

key role in cognitive inhibition [15]. Our findings further support the idea that β-band activity not only plays a critical role in cognitive processing, but also in emotional processing, suggesting that β-band activity is a general driver of inhibition, regardless of the type of interfering information. Likewise, the role of the IFG in cognitive processing has mainly been studied in specific subcomponents of inhibitory control [15, 34], i.e., behavioral inhibition [20]. However, our study found that rIFG is also involved in two other inhibitory subcomponents, i.e., stimulus interference inhibition (reaction time) and response inhibition (accuracy) as measured by the Flanker task. This suggests that rIFG plays a broader role in inhibitory control, not limited to specific inhibitory subcomponents. Its particular role in emotion processing is even less well studied and understood (see [10, 11, 35]). Our findings, which link activity in rIFG to both emotional and cognitive processing (i.e., emotional and cognitive interference) as well as their interaction (i.e., emotional interference inhibition), support the idea that the rIFG plays a critical general role in interference inhibition, regardless of the type of information causing the interference. Such a central role in interference inhibition is even further supported by our observation of the long-range modulation that rIFG exerts over visual and parietal areas, explaining the behavioral emotional and cognitive interference effect. Here, task-relevant cognitive top-down modulation from rIFG is beneficial for behavioral performance, whereas task-irrelevant emotional top-down modulation is detrimental. The involvement of the rIFG in interference inhibition to pursuit of a goal can be explained by the fact that this process often requires inhibition, cancelling or stopping, in conjunction with updating and shifting, which share a common (inhibitory) basis, as suggested by [4, 5]. Such a broad involvement in various processes requires large-scale interactions in the brain, with the *pars orbitalis* and *pars triangularis* showing among the rIFG subdivisions the highest level of anatomical and functional connectivity to other brain areas [10, 28]. In line with this notion, research by [36] suggested that the macaque Broadman area 45, which corresponds to the rIFG *pars triangularis*, is part of a tightly integrated large-scale innermost core network that connects various brain regions, including premotor, prefrontal, occipital, temporal, parietal and thalamic regions, as well as the basal ganglia, cingulate cortex, and insula. These connections offer both direct and indirect pathways that could explain the observed long-range top-down effects of rIFG to V2 and Precuneus serving as a basis for emotional and cognitive processes and their behavioral expression.

Top-down modulations of parietal and occipital cortices by rIFG had significant effects on behavioral performance in our study. Specifically, negative emotions had a negative impact on behavioral performance, possibly by engaging resources due to implicit emotion regulation [37], or to their increased saliency [38]. This effect was more pronounced when the cognitive load was low (congruent condition) compared to when it was high (incongruent condition). This suggests that there is competition for resources between cognitive processing and resources allocated to emotional interference (see [6, 39]), with

cognitive processing being more successful under high cognitive load. In other words, the cognitive process "won" when the load was sufficiently high, i.e., we observed a form of emotional interference *inhibition* during increased cognitive load. Hence, in order to prevent task-failing during high cognitive load, the cognitive process demands a substantial allocation of neural processing resources to ensure goal-directed and beneficial behavioral outcomes, even at the cost of resources allocated away from the emotional process. Our interpretation is that on the neural level, the rIFG plays a critical role in solving resource competition by allocating resources to either process and thereby implements a form of emotional interference inhibition. The outcome of this process is also transmitted to visual and parietal cortices via top-down modulations of V2 and Precuneus. These long-range modulations could bias visual sensory processing in favor of task-beneficial processing by reducing emotional or cognitive (stimulus) interference. This interpretation is supported by previous research indicating IFG's involvement in visual processing, such as salience [38] or change detection [40], and its potential to alter sensory processing [29, 41]. Since the IFG is also part of the attentional network, such long-range modulations and the sensory biases induced by them might involve attentional processes as well [42]. Our findings of frequency-specific top-down modulation are consistent with previous research, implicating α/β-band (see [43–46]) and (high) γ-band [47] activity in inter-regional connections, feedback, inhibitory control, attention [48] and emotional perceptual processing, respectively.

Implications for a general theory of emotion-cognition interaction

Our findings fit within Pessoa's dual competition model, where competition can arise at the perceptual and executive level [2]. Such competition due to emotion (or motivation, as he described) can both enhance and impair behavioral performance in cognitive tasks. Pessoa's framework is based, inter alia, on the limited resources theory by Norman [6], which proposes that systems have limited processing resources and must allocate them to competing processes, selecting the most relevant processes for goal-directed behavior [3, 7]. Spare capacities are used for task-irrelevant processes if resources are not fully consumed [39]. Processes will interfere only once the limited capacities of the shared common pool are exceeded [6]. However, emotional stimuli receive processing resources automatically and passively, even if irrelevant [1]. Yet, the brain must actively focus on task-relevant cognitive stimuli, displacing emotional processing. Our results reveal the spatio-temporal evolution of this shifting process at the neurophysiological and behavioral level. The shift depends on factors such as task-relevance of the emotional stimuli, threat vs. reward quality, and the level of processing where resource competition occurs (perceptual or executive) [2] as emotional processing is capacity-limited [3, 39]. Meaning that only when resources are not fully occupied, free resources are used for task-irrelevant processes [39]. Thus, the perceptual load is consequently the critical factor in determining whether distractors are perceived and require late selection and active control, or whether they are not perceived

due to early selection [39]. Even though emotional and cognitive stimuli are presented successively in our task, our observations demonstrate a competition between emotion and cognition on both the neural and the behavioral level. Regarding behavioral performance, Pessoa states that task-relevant stimuli typically improve performance, while task-irrelevant stimuli impair it by diverting resources away from the task. Our experiment corroborates this notion, as task-irrelevant emotional stimuli (negative images) impaired behavioral performance, as seen in slower reaction time and lower accuracy, i.e., showed an emotional interference effect. The emotional interference was stronger in low cognitive load conditions. This finding can be explained by the reallocation of executive processing resources from task-irrelevant emotional stimuli to the task-relevant Flanker stimulus when cognitive load is high. With more executive resources occupied by the high cognitive load, there are fewer resources available for late processing of emotional stimuli, reducing the emotional interference effect. On the neural level, according to Pessoa's model, the ACC is identified as a key brain region mediating the interaction between emotion/motivation and executive functions [2]. The ACC is known for its involvement in conflict monitoring [49, 50], but also cognitive and emotional processes [12, 13]. However, our study found that although the ACC was affected by the emotional interference, as it showed main effects of emotion during Flanker stimulus presentation (i.e., tROI Flanker), it did not show a significant emotion-cognition interaction effect, and therefore is not involved in emotional interference inhibition. The rIFG, on the other hand, showed significant interaction effects and thus may play a more crucial role in emotional and cognitive processing and might serve as a common resource pool besides the ACC in our task. However, the amygdala, which Pessoa considers to have a central role in his model based on its extensive connectivity, did not show significant effects at all in our study. This may be due to the difficulty of reconstructing subcortical regions with EEG and FEM models, or due to our conservative statistics. Our study supports the dual competition model of [2] by showing the involvement of the rIFG in both inhibiting task-irrelevant emotional processing and shifting attention towards task-relevant stimuli, i.e., employing emotional interference inhibition. The results of our study suggest that the rIFG serves as an executor of shifting (see also [4]) and inhibition at the intersection of executive functions and emotion processing, as evidenced by the interaction effects found in the rIFG. On the perceptual level, a competition may occur if lingering effects of emotional images interfere with Flanker stimuli. Other previous studies indicate that perceptual competition occurs in visual cortex, as emotions enhance sensory representations here [8, 51], which is in accordance to our findings of an emotion-cognition interaction effect in the high γ band in Precuneus and V2. This indicates that emotional interference in such regions requires emotional interference inhibition executed by rIFG that regulates activity in Precuneus and V2 via top-down modulations. These top-down modulations by rIFG might serve as a regulatory mechanism to counter-balance automatic processing effects of emotional stimuli or bias

visual processing. Thus, the re-distribution of perceptual resources might be driven by executive processes in rIFG. These results provide empirical support for the dual role of the IFG described in Pessoa's model, and detail the competition of emotion and inhibition as one executive process. Specifically, our results underscore the pivotal role of IFG in this interaction and shed light on the specific brain regions, timing, frequency, and connectivity involved. In conclusion, our study supports and extends Pessoa's model, providing new insights into the underlying neural mechanisms of emotion-cognition interaction.

Why does resource competition have large behavioral effects when seemingly less resources are needed overall?

Some readers may find it counter-intuitive that resource competition is considered the source of emotional interference, and yet the effect of this interference seems to be larger in the behavioral performance when the competition for resources seems to be weak, i.e., in the low cognitive load condition. While our observations do indeed fit with established theories, we would like to give a more detailed explanation here. There are actually two potential explanations for our observations within the above theoretical framework: First, it could be that there is simply not enough pressure to "solve the competition" in the condition with low cognitive load. Thus, both processes get resources, whereas the actual need to assign resources predominantly to the cognitive process, i.e., to employ emotional interference inhibition, is greater in the high load condition where failing is more likely. In other words, even though there is a larger emotional interference during low cognitive load (congruent condition), the task is still sufficiently well solved; there is even a behavioral ceiling effect in that condition. Second, as reaction times are slower (and accuracies lower) in the high cognitive load (incongruent) condition there is more time to employ emotional interference inhibition and to modulate the final emotional impact on the behavior, whereby the emotional interference effect is reduced in this condition.

Potential Clinical Implications

Impairment to control interfering impulses, whether cognitive or emotional, is a hallmark of various psychiatric disorders, including attention-deficit-hyperactivity disorder [52], autism [53], borderline personality disorder [54], major depression [55], obsessive-compulsive disorder [56], or substance use disorder [57]. Of note, recent research by [20] suggests that different subtypes of interference control are operative in different psychiatric disorders, implying that these constructs may not be universally applicable. In contrast, findings from our current study show that both stimulus and response interference inhibition are affected by emotional interference. Further research is thus needed to elucidate the exact endophenotypes and pathophysiology of (selective) impairments of inhibitory control in patients with psychiatric disorders. Our study found evidence of the involvement of the rIFG, specifically the *pars triangularis*, in emotional interference inhibition. Previous research has linked

aberrant neural activation patterns in IFG to anxiety and depression [58] and obsessive-compulsive disorder [59], and suggests that rIFG is a convergent site for response inhibition and state anger [60]. Likewise, reduced rIFG activity was reported in the context of impaired emotional interference inhibition in patients with major depressive disorder [61]. Taken together, these and our own findings highlight the critical role of rIFG in emotional interference inhibition and its potential as a target structure for therapy of mental disorders. The temporal and frequency information provided by our current study could guide development of targeted interventions, e.g., by non-invasive (electric or magnetic) brain stimulation [62, 63]. However, further research in patients with psychiatric disorders is clearly needed to elucidate the neural mechanisms of dysfunctional emotion-cognition interaction with similar spatio-temporal precision as in this study, thus potentially identifying neural targets for engaging and modulating rIFG and its subregions for treatment of impaired inhibitory control in these disorders. In addition to the importance for pathological conditions, our results will inform future preventive interventions for self-regulation and resilience fostering [64].

4 Conclusion

In summary, our study provides compelling evidence for the importance of the rIFG, particularly the *pars triangularis*, in the interaction between emotion and cognition. By determining this interaction in space, time, frequency, and information transfer with high spatial and temporal resolution, we have shed new light on the neurophysiological mechanisms underlying emotional and cognitive processing, and the crucial role of rIFG in emotional interference inhibition. Overall, our study contributes to a more integrated understanding of the interplay between emotion and cognition, with clinical implications for psychiatric disorders such as depression and substance abuse.

5 Methods

Ethics information

The study and all experimental protocols were approved by the local ethics committees of the Medical Board of Rhineland-Palatinate, Mainz, Germany, and Johann Wolfgang Goethe-University, Frankfurt, Germany, (ethical approval: 837.074.16(10393)) and all participants were financially compensated for study participation.

Participants

A total of 121 healthy human subjects participated in this dual-center study after written informed consent (i.e., 59 and 62 subjects at study sites Frankfurt and Mainz, respectively). All participants were screened for magnetic

resonance imaging (MRI) exclusion criteria, mental health status (Mini-International Neuropsychiatric Interview [65]) and handedness (Edinburgh Handedness Inventory [66]) prior to study inclusion. Four participants had to be excluded due to technical failures of the stimulus presentation during task performance. The data of the remaining 117 subjects were used for the behavioral analysis. Another thirteen participants were excluded from electrophysiological analysis due to missing or incomplete MRI data sets (three subjects due to panic attacks in the MR scanner which led to a premature abortion of the measurement, one subject due to pain during MRI measurement which led to a premature safety abort of the measurement, one subject did not fit into the MR scanner due to excessive abdominal girth, and eight subjects withdrew study consent before MRI measurements took place) and one subject had to be excluded due to external noise during EEG recording which could not be controlled for. Thus, all presented electrophysiological data are from analyses of the remaining 103 participants (65 females; mean age $\pm$ SD, 25 $\pm$ 6 years), who completed the study.

Questionnaires

After study inclusion and screening for MRI exclusion criteria (see above), participants completed questionnaires on demographic information (Gender, date, and place of birth, family origin, psychological diseases within the family, family tree, marital status), Health and Lifestyle (physical and mental diseases, height and weight, blood pressure, medication, usage of internet, working conditions, income, family relationships, MRI compatibility) and their drug consumption (Fagerström for nicotine consumption and the AUDIT for alcohol consumption) (secutrial, www.secutrail.com). Further questionnaires were the Trier Inventory for the Assessment of Chronic Stress (TICS), the Short Form 36 Health Survey Questionnaire, the General Health Questionnaire (GHQ-28), the Life events checklist from LHC (adapted from [67]), the Cognitive Emotion Regulation Questionnaire (CERQ), the Positive and Negative Affect Schedule (PANAS), the State-Trait Anger Expression Inventory (STAXI), the State-Trait Anxiety Inventory (STAI), the Barratt Impulsiveness Scale (BIS-11 [68]), the Behavioral Activation and Behavioral Inhibition Scales (BIS/BAS), the Edinburgh Handedness Inventory [66] and an Intelligence test (L-P-S Leistungsprüfsystem UT-3 [69]).

Experimental Design

Data collection took place in Frankfurt (Site 1) and Mainz (Site 2), respectively. At Site 1, 59 participants and at Site 2, 62 participants took part in the experiment. We attempted to set up and standardize the procedures as closely as possible. The experiment comprised of three experimental days (Day 1-3), two EEG measurements (Day 1 and 2) and one fMRI measurement (Day 3). On Day 1, participants were screened for exclusion criteria (see subsection Participants). Additionally, on Day 1 and 2, participants filled out the study

questionnaires (see subsection Questionnaires). In total, four different behavioral paradigms (emotional Stop stimulus Task, emotional Recent Probes Task, Cognitive Emotion Regulation Task and emotional Flanker Task) were performed by the participants on Day 1 and 2, with two tasks being performed per experimental day [FMD: order of tasks randomized across subjects? / OT: counterbalanced across subjects?]. For each task, the order of the trials was counterbalanced within and across participants. During execution of the tasks, an electroencephalography (EEG), which was spatially localized using digitalized electrode localization and finite element head models (see Finite element head modeling (FEM)), was recorded simultaneously. In addition to task-related EEG, an eyes-closed resting state EEG (rsEEG, 10 min) was recorded, either on Day 1 or Day 2 prior to task-related recordings, with the order of rsEEG on Day 1 or Day 2 counterbalanced across subjects. On Day 3, a resting state fMRI as well as structural T1 and T2 MRI measurements were carried out on each participant. Here, only data from the emotional Flanker Task EEG recordings as well as structural MRI measurements will be reported (see Structural imaging and head modelling and Electroencephalography – recording and analysis).

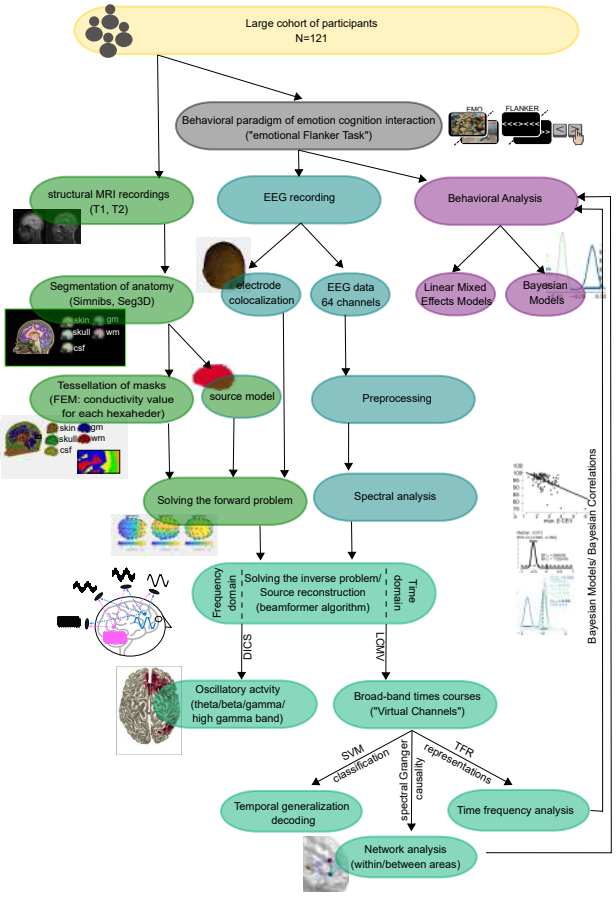

Fig. 10 Pipeline for the analysis of emotion-cognition interaction. All major analysis steps are shown in the pipeline including EEG source reconstruction with Finite Element Headmodeling Finite element head modeling (FEM) based on digitalized electrode positions Electrode digitalization and spatial localization, structural analysis Structural imaging and head modelling and beamforming Source analysis, non-parametric statistics on source level Statistical analyses of source reconstruction results, temporal generalization of sources Temporal Generalization of condition classification, and Granger Causality analysis of information transfer between neural sources Integration and segregation of emotional and cognitive information within IFG, Non-parametric Granger Causality Analysis and behavioral analysis Bayesian analysis of behavioral data Bayesian correlation of min/-max β power interaction values with behavioral measures,Bayesian linear regression of β power with behavioral measures, Correlation of top-down Granger Causality with behavior.

Task Design

For testing cognitive processing (i.e., stimulus interference and response selection interference operationalized by reaction time and accuracy, respectively, [20]) in the context of emotional distraction, a custom-made modified version of the Eriksen Flanker Task [70] was used, which was implemented in Presentation® (Version 18.1, Neurobehavioral Systems, Inc., Berkeley, CA, www.neurobs.com). Specifically, the Flanker stimulus in each trial was preceded by a picture with either neutral or negative emotional valence, taken from the International Affective Picture System (IAPS, [71]). Each trial consisted of (see Fig. 1 A): fixation cross (central, on black background, duration: 1000 ms), emotional stimulus (IAPS picture, neutral and negative, duration: 500 ms) and Flanker stimulus (white arrows on black screen, with congruent or incongruent flanking arrows, duration: 1000 ms). The inter-trial interval (black screen) was 400 ms. Participants were instructed to indicate the direction of the central target arrow via left or right button presses (i.e., left and right ctrl buttons on regular keyboard) via the index finger of the respective hand and ignore the flanking arrows. In case of an incorrect (wrong button press) or a response that was too slow (reaction time $>$ 1000 ms) an error/no response feedback was displayed on the screen for 300 ms. In total, 1120 trials in five blocks of 224 trials each (duration: 11 min) were performed during simultaneous EEG recording. IAPS pictures were used as emotional stimuli: 280 neutral pictures (mean valence was 5.15, mean arousal was 3.17) and 280 negative pictures (mean valence was 2.47, mean arousal was 6.41). Each emotional picture was repeated twice and with different Flanker stimulus. The combination of the emotional stimulus (negative/neutral) followed by the Flanker stimulus (incongruent/congruent) led to four different conditions, i.e., neural congruent: neutral picture followed by congruent Flanker, neutral incongruent: neutral picture followed by incongruent Flanker, negative congruent: negative picture followed by congruent Flanker, and negative incongruent: negative picture followed by incongruent Flanker. For each condition, 280 trials were presented with half of the trials showing a right- and left-side directed central target arrow, respectively. Blocks of trials were separated by 5 minutes to allow participants to relax in between blocks. To familiarize subjects with the task, prior to the recording, a training block with 20 trials with neutral pictures only was presented at the beginning of the experiment.

Behavioral Response acquisition

Behavioral responses were analyzed in terms of reaction time and accuracy. Reaction time was measured as the time in ms after the Flanker stimulus onset until the button press of the subject. Only correct trials were considered for reaction time analysis. Reaction times faster than 90 ms were excluded, as reaction times in this range have been reported to be biologically implausible [72, 73]. Trials with a reaction time above 1000 ms were excluded too. Accuracy was determined as the ratio of all correct trials and all displayed trials of a given

task condition, and calculated for each condition separately. The statistical analysis was performed on 117 subjects (see above).

Bayesian analysis of behavioral data

The experimental effect of the factors emotion and cognition on reaction time and accuracy was determined with a Bayesian linear regression. We employed a hierarchical model and used a non-centered parameterization [74, 75] to foster convergence. We modelled the emotion and cognition effects and their interaction. For comparison to previous studies using frequentist statistics a similar mixed-effect model was also analyzed [76] with (RStudio Version 1.4.1106 © 2009-2021 RStudio, PBC); the corresponding mixed-effects modeling procedures and results are reported in the Supplementary information about behavioral effects of emotion-cognition interaction and Tab. A1. In the following, we describe the Bayesian model definition for reaction time and accuracy data. Single-trial values of reaction times were z-transformed and log-transformed (to account for their skewed distribution) before fitting the model, the estimated regression coefficients are reported with respect to these transformations. For the ith trial and the jth subject, we can define the likelihood of the reaction time given by $y_{i,j}$ as:

$$y_{i,j} \sim \mathcal{N}(\alpha_j + x^E_{i,j}\beta_{1j} + x^C_{i,j}\beta_{2j} + x^E_j * x^C_j\beta_3, \sigma^2) \tag{1}$$

where for the jth subject, α_j is the random intercept and encodes the grand average response time and β_{1j}, β_{2j} are the random slopes which capture the differences in response times for emotion (negative vs. neutral), cognition (incongruent vs. congruent), respectively. Adding per-subject random slope parameters also for the interaction predictor term β_3 did not improve the model and was thus left out. The term $x^E_{i,j}$ encodes the emotion condition (-0.5 = negative; 0.5 = neutral), the term $x^C_{i,j}$ encodes the cognitive condition (-0.5 = incongruent; 0.5 = congruent). To obtain a more efficient sampling of the posterior, we inferred the random effects (intercepts and slopes) with a deterministic transformation of the parameters α_j and $\beta_{1..2j}$. More specifically, we did not infer individual slopes by modeling their values directly, for example saying that they are normally distributed around a group mean. Instead, we modelled their values relative to the mean (i.e., β_{offset}) and allowed the effects to deviate from the mean to a certain degree (i.e., σ_b).

$$\alpha = \alpha_{intercept} + \alpha_{offset} * \sigma_a \tag{2}$$

$$\beta_1 = \beta^E + \beta^E_{offset} * \sigma_{b^E} \tag{3}$$

$$\beta_2 = \beta^C + \beta^C_{offset} * \sigma_{b^C} \tag{4}$$

$$\tag{5}$$

For the accuracy data we assumed $Y_{i,j}$ to have a Bernoulli distribution:

$$y_{i,j} \sim Bernoulli(p) \tag{6}$$

with probability of success p_i, where in the logistic regression model the logit of the probability p_i is a linear function of the predictor variable x_i:

$$logit(p_i) = \alpha_j + x^E_{i,j}\beta_{1j} + x^C_{i,j}\beta_{2j} + x^E_j * x^C_j\beta_3, \sigma^2 \ . \tag{7}$$

As above, we used the same non-centered parameterization. All parameters were assumed to be drawn from normal distributions. We used non-informative priors in both models that can be found in Tab. A3.

Structural imaging and head modelling

Electrode digitalization and spatial localization

The position in space of all electrodes as well as the location of the nasion and fiducials were digitized and recorded with the ultrasonic sensor pen 3D-Digitizing System ELPOS and the respective ElGuide Software (ZEBRIS, Zebris Medizintechnik, Tübingen, Germany). Care was taken to ensure correct registration and spatial configuration of the electrodes. To this end, we created an average configuration file for each EEG cap size (56 cm, 58 cm, 60 cm) of all participants wearing the respective cap size. We then compared each electrode position of each individual electrode configuration to i) the respective electrode position of the average electrode configuration and ii) to the respective electrode position of the same participant's electrode configuration at her/his second EEG session (not of interest for this study) via Euclidean distance. In case an electrode position exceeded 1 cm off reference, we replaced its position with the respective coordinates of either the average configuration or of the second EEG session configuration, depending on visual inspection to ensure correct electrode position.

Magnetic resonance imaging (MRI)

To create individual head models for source reconstruction, T1- and T2-weighted structural MRI datasets were acquired for each individual participant. To ensure later co-registration and alignment of the digitized electrode position, fiducials were used as anatomical markers. We added vitamin E pills at the fiducials positions when acquiring the MRI, using the same convention when marking them during the digitization of the electrodes' location. At the study site 1 (Frankfurt), MRI data were acquired at a SIEMENS MAGNETOM Trio Syngo MR A35 3 Tesla MRI System (Erlangen, Germany) with an 8-channel head coil. A magnetization prepared rapid gradient echo (MPRAGE) T1-weighted sequence with fat suppression lasting 4:28 min (192 sagittal slices of 1 mm thickness with a distance factor of 50%, FOV 256 × 256 mm, 256 × 256 matrix, TR = 1900 ms, TE = 2.74 ms, flip angle = 9°, 1.0 × 1.0 ×

1.0 mm3 voxels) and a turbo spin-echo sequence (TSE) sequence lasting 7:51 min (192 sagittal slices of 1 mm thickness with a distance factor of 0%, FOV 256 × 256 mm, 256 × 256 matrix, TR = 1500 ms, TE = 355 ms, flip angle = 0°, 1.0 × 1.0 × 1.0 mm3 voxels) were acquired. At study site 2 (Mainz), MRI data were acquired at a SIEMENS MAGNETOM TrioTim Syngo MR B17 3 Tesla MRI System (Erlangen, Germany) with a 32-channel head-coil. The specific parameters for each sequence were defined to match as closely as possible those from study site 1 given the respective specificities of the MRI system and the available software. That is, an MPRAGE T1-weighted sequence with fat suppression lasting 4:26 min (192 sagittal slices of 1 mm thickness with a distance factor of 50%, FOV 256 × 256 mm, 256 × 256 matrix, TR = 1900 ms, TE = 2.23 ms, flip angle = 9°, 1.0 × 1.0 × 1.0 mm3 voxels) and a TSE sequence lasting 7:50 min was used (192 sagittal slices of 1 mm thickness with a distance factor of 0%, FOV 256 × 256 mm, 256 × 256 matrix, TR = 1500 ms, TE = 339 ms, flip angle = 0°, 1.0 × 1.0 × 1.0 mm3 voxels) were used.

Finite element head modeling (FEM)

To create individual finite element head models, we used SimNIBS (Version 2.0.1, www.simnibs.org) with mri2mesh [77] and the FieldTrip-SimBio pipeline (Version 2.0.1) [78]. First, the mri2mesh pipeline from SimNIBS was used with the individual T1 and T2 images as input to create realistic individual segmentations. Hereby T2-weighted images, in addition to T1-weighted images, are used to further improve the segmentation between skull and cerebrospinal fluid [79]. This pipeline involves Freesurfer [80, 81] and FSL [82] to automatically segment brain and non-brain tissue into five compartments (skin, skull, cerebrospinal fluid, white, and gray matter) [77]. The results of the automatic segmentations were visually inspected in Seg3D (version 2.2.1, Scientific Computing and Imaging Institute, University of Utah, https://www.sci.utah.edu/cibc-software/seg3d.html) to check for segmentation errors and manually correct them if necessary. The surface masks so generated were checked for holes and overlaps. Using the Fieldtrip-Simbio pipeline, the masks were then transformed into meshes consisting of hexahedrons, which subsequently were used to compute the individual FEM forward solutions. Following [83, 84] we assigned 0.33, 0.14, 1.79, 0.01 and 0.43 S/m as conductivity values for gray matter, white matter, cerebrospinal fluid, skull, and scalp. The FEM models were aligned to the digitized electrode positions via the nasion and fiducials. To reduce the space between the real recording site (lower part of the electrode) and the digitized site (upper part of the electrode), the electrode position of each electrode was projected down to the nearest point onto the skin. We warped a 3-D template grid with 10 mm spacing in Montreal Neurological Institute (MNI) from fieldtrip [85] to each individual head model covering the whole brain. Hereby, each grid point can directly be compared to the same grid points of other participants, as each point represents the same respective brain area. As a last step, we calculated

the individual lead fields per warped grid point, representing the electrical field of the respective tissue, given the individual electrode position.

Electroencephalography – recording and analysis

Data acquisition

Surface EEG was continuously recorded during the emotional Flanker task with an active 64-channel EEG system (actiCAP system, Brain Products GmbH, Gilching, Germany) using the standard 64Ch-actiCAP-Slim electrodes montage (Brain Products GmbH, Gilching, Germany). Four recording channels (predefined in the montage by brain products at position P7, P8, P9, P10) were placed near the outer right and left edges of the eye and 1 cm below and above the right eye to collect horizontal and vertical electrooculography (EOG), respectively. Therefore, EEG data was collected from only 60 channels. EEG data were recorded with BrainVision Recorder (Version 1.20.0601) with a sampling rate of 2.5 kHz, except for the first nine participants at Site 1, where a sampling rate of 5 kHz was used. Participants were placed centrally at about 80 cm distance in front of a standard PC monitor (ASUS VG278HV, 27", 144Hz, 1920×1080, 1 ms GTG) within an EEG chamber with sound and RF shielding. In order to minimize artifacts during data acquisition, participants were instructed to relax their jaw and neck muscles and sit as still as possible during the recordings.

Preprocessing of EEG data

Preprocessing and analysis of the EEG data were performed with MATLAB R2012b (MathWorks Inc, Natick, MA, USA) and the FieldTrip toolbox (Version 20180729) [85]). First, data were low-pass filtered with a cut-off at 300 Hz. Subsequently, data were down-sampled to 500 Hz and cut into 1500 ms long epochs starting with the emotional picture onset. Other epochs were cut 2000 ms starting with the fixation cross onset and ending 500 ms after Flanker stimulus onset. Bad trials (i.e., with electrode jumps or muscle artifacts) were rejected using the FieldTrip automatic artifact rejection functions and line noise was filtered out with discrete Fourier transform filters at 50, 100, 150 and 200 Hz. Further artifacts (e.g., due to eye movements or heart beat) were removed using an extended infomax (runica) algorithm (provided in Fieldtrip/EEGLAB) [86]. Independent components were visually inspected and rejected based on topography and spectral power [87] and/or if there was a significant correlation (rho> 0.3) with either the EOG stimulus or with a prototypical "square-root" spectrum commonly observed in muscle artifacts [88]. Then data was re-referenced to the common average. This EEG data cleaning approach resulted in, on average, exclusion of 16.29 ± 29.72 (mean ± standard deviation) trials (range of excluded trials 0 to 177) out of a total of 1120 trials. To assure that statistical differences in subsequent comparisons were not caused by different numbers of trials per condition, we stratified the number of trials per condition per subject by randomly selecting for each condition the

minimum amount of trials found across conditions in case of differences in the number of trials per condition. Furthermore, we only used correct trials, i.e., trials with correct button presses within required response times ($>$ 90 ms, $<$ 1000 ms).

Spectral analysis at sensor level

To define specific frequency bands for subsequent source reconstruction and further source-level analysis (see Source analysis), we first analyzed the spectral power at sensor level in order to find all potentially task relevant frequency bands. We obtained spectral power estimates between 3 and 120 Hz with Hanning tapers, over the tROI Flanker, and baseline period (see Temporal ROI definition), for all EEG channels and participants. In order to avoid circular reasoning and 'double-dipping' with respect to the subsequent statistical analysis comparing conditions in EEG source space, we performed sensor-level statistics by contrasting 'pooled' task conditions (all four conditions) with corresponding baseline periods ([89]). For this, we used a dependent samples t-test and a cluster-based correction method ([90]) to account for multiple comparisons across frequencies only (since data was averaged across channels and time). We employed a two-tailed test with an alpha threshold of $\alpha = 0.025$ and cluster alpha of $\alpha_{cluster} = 0.025$. Finally, to delineate different frequency bands in the statistical analysis results, we identified the points of maximum curvature in the t-value vs. frequency curve by visual inspection. This allowed us to determine four non-overlapping frequency bands (a θ band from 5 to 9 Hz with a center frequency of 7 Hz ($\pm$ 2 Hz spectral smoothing), a β band from 9 to 33 Hz with a center frequency of 21 Hz ($\pm$ 12 Hz spectral smoothing), a γ band from 33 to 64 Hz with a center frequency of 49 Hz ($\pm$ 16 Hz spectral smoothing) and a high γ band from 64 to 140Hz with a center frequency of 102 ($\pm$ 38 Hz spectral smoothing) (see Fig. A1).

Temporal ROI definition

Two temporal regions of interest, one during the Flanker stimulus presentation (tROI Flanker) and another during the emotional picture presentation (tROI Emo) were defined 1 for each frequency band. To exclude early visual processing, the tROI Flanker started only 50 ms after the Flanker stimulus onset ([91, 92] and ended around the average minimum reaction time (430 ms) to exclude motor responses. This led to time windows of interest for each frequency band (beta, γ, and high γ band) with a duration of approximately 380 ms. The duration of tROIs varied slightly to match a full number of cycles of the center frequency of each frequency band, i.e., a center frequency of 21 Hz in the beta band resulted in a tROI of 380.95 ms (8 full cycles), a center frequency of 49 Hz in the γ band resulted in a tROI of 387.76 ms (19 full cycles) and a center frequency of 102 Hz in the high γ band resulted in a tROI of 382.35 ms (39 full cycles). As lower frequencies have longer wavelengths, we increased the time window for the θ band to obtain three full cycles of the center frequency of 7 Hz to 428.57 ms by starting at tROI FLANKER onset.

The same procedure was applied to the tROI EMO during the emotional picture presentation. In the θ band, analogous to the tROI FLANKER, the tROI EMO was 428.57 ms long and started at the emotional picture onset; see Fig. 1 B and Temporal ROI definition for definition of tROIs).

Source analysis

Beamformer source analysis was performed using the dynamic imaging of coherent sources (DICS) algorithm [93], with real-valued filter coefficients, as implemented in FieldTrip. This adaptive spatial filter estimates the power at each grid point based on individual lead fields (see Finite element head modeling (FEM)) and cross-spectral density matrices. The latter were computed for the two previously described ROIs (see Temporal ROI definition for further details) and for a baseline period (from -500 ms to -120 ms (and to -71.65 ms in the case of θ) before the onset of the emotional picture during the fixation cross) and four different bands. The frequency bands were defined as described in section Spectral analysis at sensor level, and consisted of a θ band with a center frequency of 7 Hz ($\pm$ 2 Hz spectral smoothing), a β band with a center frequency of 21 Hz ($\pm$ 12 Hz spectral smoothing), a γ band with a center frequency of 49 Hz ($\pm$ 16 Hz spectral smoothing) and a high γ band with a center frequency of 102 ($\pm$ 38 Hz spectral smoothing). Cross-spectral density matrix calculation was performed using the FieldTrip toolbox with the multitaper method [94]. We used a regularization of 5% ([95]). Beamformer filters were computed based on the data from both tROIs and the baseline across all conditions ('common filters'), thus assuring that differences in source activation do not arise from differences in filters derived from the individual conditions. Additionally, we report point estimates (mean) and 95% confidence intervals from bootstrapping with 5000 random resampling for each contrast: emotion (negative − neutral), cognition (incongruent − congruent) and emotion-cogniton interaction ((negative incongruent − neutral incongruent) − (negative congruent − neutral congruent)).

Statistical analyses of source reconstruction results

The source statistics comprised of two levels. First, we computed within-subject t-values by two-sided t-tests on single trial data for tROI Flanker versus baseline and for tROI Emo versus baseline (see Fig. 1) for each task condition and grid point (dual state beamformer [96]) with an alpha of 0.025. Second, a 2x2 repeated-measures cluster permutation ANOVA [97] (for code see https://github.com/sashel/permANOVA) with the within-subject factors emotion (negative/neutral) and cognition (incongruent/congruent) was performed on t-values obtained from the first level, across subjects. To correct for multiple comparisons in four frequency bands (θ, β , γ and high γ) and two time windows (tROI Emo and tROI Flanker) we used Bonferroni correction with a factor of 8 leading to an alpha level of 0.00625. To correct for the number of grid voxels, we used a cluster-based correction approach [90] with 5000 permutations and a cluster-alpha level of 0.00625. Further, we obtained the

coordinates of the active sources using the local maxima of the activation – without resorting to prior assumptions on their locations. This approach is in line with best practices recommendations for source reconstructions in MEG [98].

Temporal Generalization of condition classification

We used a time-resolved support vector machine analysis (t-SVM) with a linear kernel to test the ability of a classifier trained at each time sample to discriminate conditions at all other time samples [99] on source activity time courses as input data. The t-SVM was trained and tested separately for each subject, and each IFG subregion (IFG_{Tri}, IFG_{Op} and IFG_{Orb}). First, we z-normalized each source activity time course relative to the baseline period (see Temporal ROI definition for definition of baseline). Then, we smoothed the data with a Gaussian Kernel of ±25 ms and down sampled it to 250 Hz, similar to the approach in [100], and low-pass filtered at 60 Hz, in order to reduce the computational cost and increase the stimulus-to-noise ratio. After preprocessing, the source data were randomly assigned to one of twenty *supertrials* (per condition) and averaged (MATLAB code was adopted from [101], which builds on the library for SVMs by [102]). Finally, we separated these *supertrials* into training and testing data, with one *supertrial* per condition serving as test data and all others as training data. The binary classification was performed for each time point from 0 ms to 1000 ms after the onset of the emotional picture. Training one classifier at time t and generalizing it to time t' was performed within the cross-validation so that t and t' data came from independent sets of trials. To obtain a more robust estimate of the classification accuracy, we performed 200 iterations of *supertrials* creation, averaging and classification. The final temporal generalization classification reflects the average across these iterations. Classification for the emotional effects was performed between negative and neutral conditions, for cognitive effects classification was performed between incongruent and congruent and for the emotion-cognition interaction effects classification was performed between the pooled conditions of incongruent negative and congruent neutral versus the pooled conditions of incongruent neutral and congruent negative. This allowed to create two conditions with pooled data reflecting the interaction effect and thereby be classified with an SVM. For statistical testing, we employed a dependent-samples permutation t-test and a cluster-based correction method [90], where the number of permutations was set to 10000. The null hypothesis of no experimental effect for the two-dimensional classification matrix was equal to 50% chance level and tested within a tROI of 1000 ms including the emotional picture presentation and 500 ms of the Flanker stimulus presentation (tROI EMO and tROI Flanker) for the E contrast, while during the tROI Flanker for C and EC contrasts. The statistical tests were two-sided (the α value was set to 0.025) and Bonferroni corrected for the number of tests performed (nine tests; three IFG regions by three classifications: E, C and EC). Since the results of statistical analyses are random variables themselves, we additionally conducted bootstrapping of

the cluster parameter estimates to obtain confidence intervals. Specifically, we calculated bootstrap-confidence intervals for maximum classification accuracy and the respective time by running the cluster statistics with 5000 bootstrap samples. We calculated point estimates (mean) and 95% confidence intervals from these bootstrap samples.

Bayesian correlation of min/max β power interaction values with behavioral measures

Based on the source reconstruction and temporal generalization results (see Source analysis) we focused the subsequent analysis on $\mathrm{IFG_{Tri}}$ activity. To determine its behavioral relevance, we calculated the interaction effect ((negative incongruent − neutral incongruent) − (negative congruent − neutral congruent) in the β-band ((9−33 Hz, 0.05−0.43 ms, similar frequency and time range as for the source reconstruction, tROI Flanker). Since the magnitude of an interaction is proportional to its absolute value, the closer the interaction value is to zero, the weaker the interaction is, while the farther away it is from zero, the stronger the interaction is. This means that both minimum and maximum interaction values reflect the strongest interaction present. As we were specifically interested in individual effects of emotion-cognition interaction, we searched for the minimum and maximum β power interaction values for each subject respectively correlated them to behavioral measures (average reaction time and average accuracy per subject). We performed two-sided Bayesian correlations (Pearson's correlation) using their JASP implementation [103], regressing behavioral parameters on β-band spectral-power interaction-values. Hypotheses tested were H_0: $\rho = 0$, which is a standard setting in JASP (see http://static.jasp-stats.org/Manuals/Bayesian_Guide_v0.12.2.pdf), and H_1: $\rho \neq 0$. The standard settings of JASP for the beta priors were used to give all correlations between -1 and +1 an equal prior probability, i.e., a stretched beta prior width of 1 (see Tab. A6).

Bayesian linear regression of β power with behavioral measures

We used Bayesian linear regressions to determine the most informative factor for behavioral measures: mean β power, β power interaction, or β power interaction in relation to emotion or cognition. In the following, we describe the respective Bayesian model definitions for predicting mean reaction time and mean accuracy data based on β power values per subject. We define the likelihood of the reaction time or the accuracy respectively (given by y), denoted as:

$$y_j \sim \mathcal{N}(\alpha + mean_{power}^{min/max} + \beta_1 * \beta_{j,powerE}^{min/max} \beta_2 * \beta_{j,powerC}^{min/max} \beta_3 * \beta_{j,powerEC}^{min/max}, \sigma^2) \tag{8}$$

where for the jth subject, α is the intercept and encodes the grand average of reaction time or accuracy, the $mean_{power}^{min/max}$ is the average power over conditions and β_1, β_2 and β_3 are regression coefficients capturing the influence

of differences in $\beta_{power}^{min/max}$ for emotion (E, negative − neutral), cognition (C, incongruent − congruent) and the interaction emotion-cognition (EC, (negative incongruent − neutral incongruent) − (negative congruent − neutral congruent)), respectively. We z-normalized all variables before modeling, and β coefficients are reported with respect to these standardized variables. All parameters were assumed to be drawn from normal distributions. We used non-informative priors in both models that can be found in Tab. A8.

Non-parametric Granger Causality Analysis

To compute conditional Granger Causality (cGC), we employed a multivariate non-parametric spectral matrix factorization. We computed the CSD matrix of the source stimulus using a fast Fourier transform in combination with multitapers (5 Hz smoothing). We used the non-parametric variant of cGC [104] in order to avoid choosing a multivariate autoregressive model order, which can introduce a bias. Additionally, we used a block-wise approach [105] considering the first two principal components (PCs) of each source stimulus as a block, then estimating the cGC that a source X exerts over a source Y conditional on the remaining areas [44]. We applied the cGC to the three IFG subdivisions (IFG_{Tri}, IFG_{Orb} and IFG_{Op}) and the posterior sources that showed significant interaction effects: V2 and Precuneus (High γ band). We focused on bidirectional connectivity within IFG (IFG_{Tri}, IFG_{Op} and IFG_{Orb}) and of each IFG subdivision and V2 and Precuneus, respectively, in the post cognitive stimulus window (0.05 to 0.500 s). To alleviate the problem of non-stationarity we computed the cGC over two shorter time windows with 250 ms duration, with a spectral resolution of 2 Hz. The two time-sliding windows had an overlap of 50 ms: from 50 to 300 and from 250 to 500 ms. As the frequency ranges observed by [15] in relation to behavioral inhibition, were found to be low γ range, we broadened the statistical analysis from 10 to 44 Hz, despite our main interest lying on the β-band.

Statistical testing of cGC

First, we assessed whether the average cGC (in the frequency range of $8-44$ Hz) of the source-target pairs was reliably above the bias level for each condition (negative congruent, neutral congruent, negative incongruent and neutral incongruent) separately. In order to estimate the bias, we randomly permuted the trials 200 times in each condition to create a surrogate distribution of mean cGC values. We tested if the found cGC value was in the upper 99.37% extreme (equivalent $p<0.025$ with Bonferroni correction for four conditions) of the surrogates' distribution. If the average cGC exceeded the bias level, this source-target link was considered significant. These steps were repeated for each subject separately. Second, for both source-target pairs, we computed interaction effects on cGC values at group level on subjects showing a significant link at least in one condition. The statistical comparison was performed in the range of $8-44$ Hz using a dependent-samples permutation ANOVA. A cluster-based correction was used to account for multiple comparisons across

frequencies [90]. Adjacent frequency samples with uncorrected p-values of 0.05 were considered as clusters. Fifty-thousand permutations were performed, and the critical α value was set to 0.05. Further Bonferroni correction was applied to account for multiple comparisons across links. Additionally, we report point estimates (mean) and 95% confidence intervals from bootstrapping with 50000 random resampling for each contrast: emotion (negative − neutral), cognition (incongruent − congruent) and emotion-cogniton interaction ((negative incongruent − neutral incongruent) − (negative congruent − neutral congruent)) for each link and each significant frequency range.

Correlation of top-down Granger Causality with behavior

To understand whether the links we found are of behavioral relevance, we used Bayesian linear regressions to determine which of the significant links from IFG to visual areas is the most informative factor to predict mean reaction time and mean accuracy, respectively. In the following, we describe the respective Bayesian model definition for predicting mean reaction time and mean accuracy data based on the links that showed significant effects of emotion, cognition or emotion-cognition interaction in Granger causality at certain frequency range: For the jth subject, we define the likelihood of the reaction time or the accuracy respectively given by y; denoted as:

$$y_j \sim \mathcal{N}(\alpha + \beta_1 * cGC_j^{link_1} + ... + \beta_n * cGC_j^{link_n}, \sigma^2) \tag{9}$$

where for the jth subject, α is the intercept and encodes the grand average of reaction time or accuracy, respectively, and $\beta_1 ... \beta_n$ capture the relation between the cGC links of the IFG subdivisions to Precuneus or V2 and the dependent variables (reaction time or accuracy). Additionally, we performed Bayesian regression regressing the differences in behavioral measures (Δ^{rt} for reaction time, Δ^{acc} for accuracy) on the difference in Granger causality (ΔcGC) across links selected based on the analysis above (links that had a 94% HDI of entirely one sign). Differences between conditions were computed as incongruent − congruent, in relation to cognitive processing (c contrast), and negative − neutral for emotional processing (E contrast). In the following, we describe the respective Bayesian model definition for a regression of Δ^{rt} reaction time and Δ^{acc} accuracy data:

$$y_j^{\Delta^{rt/acc}} \sim \mathcal{N}(\alpha + \beta_1 * cGC_j^{link_1^{\Delta}} + ... + \beta_n * cGC_j^{link_n^{\Delta}}, \sigma^2) \tag{10}$$

where for the Δ^{rt} in the C contrast (incongruent − congruent) the selected *links* were the IFG_{Orb} to Precuneus and V2, while only the link IFG_{Op} to V2 entered the E contrast (negative − neutral) for Δ^{rt} and Δ^{acc} . We z-normalized all variables before modeling, and β coefficients are reported with respect to these standardized variables. All parameters were assumed to be drawn from normal distributions. We used non-informative priors in both models that can be found in Tab. A8 and Tab. A10, respectively.

Software and settings for parameter inference of Bayesian models when using Markov chain Monte Carlo sampling

Except for those cases where we indicate the use of the JASP software package, we estimated all the model regression coefficients using Bayesian inference with MCMC, using the python package PyMC3 [106] with NUTS (NO-U-Turn Sampling), using multiple independent Markov Chains. We ran four chains with 3000 burn-in (tuning) steps using NUTS. Then, each chain performed 8000 steps for the Bayesian Hierarchical model of reaction times and accuracy and 10000 steps for the Bayesian linear regression of β power and cGC values; those steps were used to approximate the posterior distribution. To check the validity of the sampling, we verified that the R-hat statistic was below 1.05.

The Bayesian Hierarchical analysis of behavioral data and Bayesian linear regression of β power and cGC values were conducted using Python (Version 3.7) [107] in Jupyter Notebook [108].

References

[1] L. Carretié, Exogenous (automatic) attention to emotional stimuli: a review. Cognitive, Affective, & Behavioral Neuroscience **14**, 1228–1258 (2014)

[2] L. Pessoa, How do emotion and motivation direct executive control? Trends in cognitive sciences **13**(4), 160–166 (2009)

[3] L. Pessoa, Précis on the cognitive-emotional brain. Behavioral and Brain Sciences **38** (2015)

[4] A. Miyake, N.P. Friedman, M.J. Emerson, A.H. Witzki, A. Howerter, T.D. Wager, The unity and diversity of executive functions and their contributions to complex "frontal lobe" tasks: A latent variable analysis. Cognitive psychology **41**(1), 49–100 (2000)

[5] N.P. Friedman, A. Miyake, The relations among inhibition and interference control functions: a latent-variable analysis. Journal of experimental psychology: General **133**(1), 101 (2004)

[6] D.A. Norman, D.G. Bobrow, On data-limited and resource-limited processes. Cognitive psychology **7**(1), 44–64 (1975)

[7] R. Desimone, J. Duncan, et al., Neural mechanisms of selective visual attention. Annual review of neuroscience **18**(1), 193–222 (1995)

[8] L. Pessoa, *The cognitive-emotional brain: From interactions to integration* (MIT press, 2013)

[9] G. Pourtois, A. Schettino, P. Vuilleumier, Brain mechanisms for emotional influences on perception and attention: What is magic and what is not. Biological psychology **92**(3), 492–512 (2013)

[10] R. Langner, S. Leiberg, F. Hoffstaedter, S.B. Eickhoff, Towards a human self-regulation system: Common and distinct neural signatures of emotional and behavioural control. Neuroscience & Biobehavioral Reviews **90**, 400–410 (2018)

[11] G. Hartwigsen, N.E. Neef, J.A. Camilleri, D.S. Margulies, S.B. Eickhoff, Functional segregation of the right inferior frontal gyrus: evidence from coactivation-based parcellation. Cerebral Cortex **29**(4), 1532–1546 (2019)

[12] G. Bush, P. Luu, M.I. Posner, Cognitive and emotional influences in anterior cingulate cortex. Trends in cognitive sciences **4**(6), 215–222 (2000)

[13] J.M. Allman, A. Hakeem, J.M. Erwin, E. Nimchinsky, P. Hof, The anterior cingulate cortex: the evolution of an interface between emotion and cognition. Annals of the New York Academy of Sciences **935**(1), 107–117 (2001)

[14] M. Xu, G. Xu, Y. Yang, Neural systems underlying emotional and non-emotional interference processing: An ale meta-analysis of functional neuroimaging studies. Frontiers in behavioral neuroscience **10**, 220 (2016)

[15] M. Schaum, E. Pinzuti, A. Sebastian, K. Lieb, P. Fries, A. Mobascher, P. Jung, M. Wibral, O. Tüscher, Right inferior frontal gyrus implements motor inhibitory control via beta-band oscillations in humans. Elife **10**, e61,679 (2021)

[16] A. Sebastian, P. Jung, J. Neuhoff, M. Wibral, P.T. Fox, K. Lieb, P. Fries, S.B. Eickhoff, O. Tüscher, A. Mobascher, Dissociable attentional and inhibitory networks of dorsal and ventral areas of the right inferior frontal cortex: a combined task-specific and coordinate-based meta-analytic fmri study. Brain Structure and Function **221**, 1635–1651 (2016)

[17] M. Goldstein, G. Brendel, O. Tuescher, H. Pan, J. Epstein, M. Beutel, Y. Yang, K. Thomas, K. Levy, M. Silverman, et al., Neural substrates of the interaction of emotional stimulus processing and motor inhibitory control: an emotional linguistic go/no-go fmri study. Neuroimage **36**(3), 1026–1040 (2007)

[18] G.A. Jacob, K. Zvonik, S. Kamphausen, A. Sebastian, S. Maier, A. Philipsen, L.T. Van Elst, K. Lieb, O. Tüscher, Emotional modulation of motor response inhibition in women with borderline personality disorder: an fmri study. Journal of Psychiatry and Neuroscience **38**(3), 164–172 (2013)

[19] D. Silbersweig, J.F. Clarkin, M. Goldstein, O.F. Kernberg, O. Tuescher, K.N. Levy, G. Brendel, H. Pan, M. Beutel, M.T. Pavony, et al., Failure of frontolimbic inhibitory function in the context of negative emotion in borderline personality disorder. American Journal of Psychiatry **164**(12), 1832–1841 (2007)

[20] C. Stahl, A. Voss, F. Schmitz, M. Nuszbaum, O. Tüscher, K. Lieb, K.C. Klauer, Behavioral components of impulsivity. Journal of Experimental Psychology: General **143**(2), 850 (2014)

[21] A. Sebastian, M. Pohl, S. Klöppel, B. Feige, T. Lange, C. Stahl, A. Voss, K. Klauer, K. Lieb, O. Tüscher, Disentangling common and specific neural subprocesses of response inhibition. Neuroimage **64**, 601–615 (2013)

[22] B. PRUESSNER, J. V. Holt, A cognitive control framework for understanding emotion regulation flexibility. Emotion **20**(1), 21–29 (2020)

[23] A. Etkin, A.F. Schatzberg, Common abnormalities and disorder-specific compensation during implicit regulation of emotional processing in generalized anxiety and major depressive disorders. American Journal of Psychiatry **168**(9), 968–978 (2011)

[24] D.M. Kronhaus, N.S. Lawrence, A.M. Williams, S. Frangou, M.J. Brammer, S.C. Williams, C.M. Andrew, M.L. Phillips, Stroop performance in bipolar disorder: further evidence for abnormalities in the ventral prefrontal cortex. Bipolar disorders **8**(1), 28–39 (2006)

[25] J.D. Bremner, E. Vermetten, M. Vythilingam, N. Afzal, C. Schmahl, B. Elzinga, D.S. Charney, Neural correlates of the classic color and emotional stroop in women with abuse-related posttraumatic stress disorder. Biological psychiatry **55**(6), 612–620 (2004)

[26] Y. Liu, Q. Fu, X. Fu, The interaction between cognition and emotion. Chinese Science Bulletin **54**(22), 4102–4116 (2009)

[27] J. Larson, T. Mavrogordatos, *The Jaynes–Cummings Model and Its Descendants: Modern research directions* (IoP Publishing, 2021)

[28] R. Boen, L. Raud, R.J. Huster, Inhibitory control and the structural parcelation of the right inferior frontal gyrus. Frontiers in Human

Neuroscience **16** (2022)

[29] C. Wang, R. Rajagovindan, S.M. Han, M. Ding, Top-down control of visual alpha oscillations: sources of control signals and their mechanisms of action. Frontiers in human neuroscience **10**, 15 (2016)

[30] J.R. Gray, T.S. Braver, M.E. Raichle, Integration of emotion and cognition in the lateral prefrontal cortex. Proceedings of the National Academy of Sciences **99**(6), 4115–4120 (2002)

[31] W.C. Drevets, M.E. Raichle, Reciprocal suppression of regional cerebral blood flow during emotional versus higher cognitive processes: Implications for interactions between emotion and cognition. Cognition and emotion (1998)

[32] T. Osada, A. Ogawa, A. Suda, K. Nakajima, M. Tanaka, S. Oka, K. Kamagata, S. Aoki, Y. Oshima, S. Tanaka, et al., Parallel cognitive processing streams in human prefrontal cortex: Parsing areal-level brain network for response inhibition. Cell Reports **36**(12), 109,732 (2021)

[33] B. Deen, N.B. Pitskel, K.A. Pelphrey, Three systems of insular functional connectivity identified with cluster analysis. Cerebral cortex **21**(7), 1498–1506 (2011)

[34] R. Hannah, A.R. Aron, Towards real-world generalizability of a circuit for action-stopping. Nature Reviews Neuroscience **22**(9), 538–552 (2021)

[35] R. Underwood, E. Tolmeijer, J. Wibroe, E. Peters, L. Mason, Networks underpinning emotion: A systematic review and synthesis of functional and effective connectivity. NeuroImage **243**, 118,486 (2021)

[36] D.S. Modha, R. Singh, Network architecture of the long-distance pathways in the macaque brain. Proceedings of the National Academy of Sciences **107**(30), 13,485–13,490 (2010)

[37] S. Padmala, A. Bauer, L. Pessoa, Negative emotion impairs conflict-driven executive control. Frontiers in Psychology **2**, 192 (2011)

[38] S. Song, A. Zilverstand, H. Song, F. d'Oleire Uquillas, Y. Wang, C. Xie, L. Cheng, Z. Zou, The influence of emotional interference on cognitive control: A meta-analysis of neuroimaging studies using the emotional stroop task. Scientific reports **7**(1), 1–9 (2017)

[39] N. Lavie, A. Hirst, J.W. De Fockert, E. Viding, Load theory of selective attention and cognitive control. Journal of experimental psychology: General **133**(3), 339 (2004)

[40] F. Verbruggen, A.R. Aron, M.A. Stevens, C.D. Chambers, Theta burst stimulation dissociates attention and action updating in human inferior frontal cortex. Proceedings of the National Academy of Sciences **107**(31), 13,966–13,971 (2010)

[41] M. Tops, M.A. Boksem, A potential role of the inferior frontal gyrus and anterior insula in cognitive control, brain rhythms, and event-related potentials. Frontiers in psychology **2**, 330 (2011)

[42] M. Corbetta, G. Patel, G.L. Shulman, The reorienting system of the human brain: from environment to theory of mind. Neuron **58**(3), 306–324 (2008)

[43] A. Bibbig, R.D. Traub, M.A. Whittington, Long-range synchronization of γ and β oscillations and the plasticity of excitatory and inhibitory synapses: a network model. Journal of Neurophysiology **88**(4), 1634–1654 (2002)

[44] A.M. Bastos, J. Vezoli, C.A. Bosman, J.M. Schoffelen, R. Oostenveld, J.R. Dowdall, P. De Weerd, H. Kennedy, P. Fries, Visual areas exert feedforward and feedback influences through distinct frequency channels. Neuron **85**(2), 390–401 (2015)

[45] A. Brovelli, M. Ding, A. Ledberg, Y. Chen, R. Nakamura, S.L. Bressler, Beta oscillations in a large-scale sensorimotor cortical network: directional influences revealed by granger causality. Proceedings of the National Academy of Sciences **101**(26), 9849–9854 (2004)

[46] T. Popov, B.U. Westner, R.L. Silton, S.M. Sass, J.M. Spielberg, B. Rockstroh, W. Heller, G.A. Miller, Time course of brain network reconfiguration supporting inhibitory control. Journal of Neuroscience **38**(18), 4348–4356 (2018)

[47] K. Yang, L. Tong, J. Shu, N. Zhuang, B. Yan, Y. Zeng, High gamma band eeg closely related to emotion: evidence from functional network. Frontiers in human neuroscience **14**, 89 (2020)

[48] K. Benchenane, P.H. Tiesinga, F.P. Battaglia, Oscillations in the prefrontal cortex: a gateway to memory and attention. Current opinion in neurobiology **21**(3), 475–485 (2011)

[49] M.M. Botvinick, J.D. Cohen, C.S. Carter, Conflict monitoring and anterior cingulate cortex: an update. Trends in cognitive sciences **8**(12), 539–546 (2004)

[50] C.S. Carter, T.S. Braver, D.M. Barch, M.M. Botvinick, D. Noll, J.D. Cohen, Anterior cingulate cortex, error detection, and the online monitoring of performance. Science **280**(5364), 747–749 (1998)

[51] P. Vuilleumier, How brains beware: neural mechanisms of emotional attention. Trends in cognitive sciences **9**(12), 585–594 (2005)

[52] J.T. Nigg, Attention-deficit/hyperactivity disorder: Endophenotypes, structure, and etiological pathways. Current Directions in Psychological Science **19**(1), 24–29 (2010)

[53] S.E. Christ, L.E. Kester, K.E. Bodner, J.H. Miles, Evidence for selective inhibitory impairment in individuals with autism spectrum disorder. Neuropsychology **25**(6), 690 (2011)

[54] J.T. Nigg, K.R. Silk, G. Stavro, T. Miller, Disinhibition and borderline personality disorder. Development and psychopathology **17**(4), 1129–1149 (2005)

[55] C.S. Carver, S.L. Johnson, J. Joormann, Serotonergic function, two-mode models of self-regulation, and vulnerability to depression: what depression has in common with impulsive aggression. Psychological bulletin **134**(6), 912 (2008)

[56] N.A. Fineberg, M.N. Potenza, S.R. Chamberlain, H.A. Berlin, L. Menzies, A. Bechara, B.J. Sahakian, T.W. Robbins, E.T. Bullmore, E. Hollander, Probing compulsive and impulsive behaviors, from animal models to endophenotypes: a narrative review. Neuropsychopharmacology **35**(3), 591–604 (2010)

[57] S.M. Groman, A.S. James, J.D. Jentsch, Poor response inhibition: at the nexus between substance abuse and attention deficit/hyperactivity disorder. Neuroscience & Biobehavioral Reviews **33**(5), 690–698 (2009)

[58] M. Serra-Blasco, J. Radua, C. Soriano-Mas, A. Gómez-Benlloch, D. Porta-Casteràs, M. Carulla-Roig, A. Albajes-Eizagirre, D. Arnone, P. Klauser, E.J. Canales-Rodríguez, et al., Structural brain correlates in major depression, anxiety disorders and post-traumatic stress disorder: A voxel-based morphometry meta-analysis. Neuroscience & Biobehavioral Reviews **129**, 269–281 (2021)

[59] B. Hollunder, J.L. Ostrem, I.A. Sahin, N. Rajamani, S. Oxenford, K. Butenko, M. Polosan, H. Akram, M. Vissani, C. Zhang, et al., Segregating the frontal cortex with deep brain stimulation. medRxiv pp. 2023–03 (2023)

[60] A.A. Puiu, O. Wudarczyk, G. Kohls, D. Bzdok, B. Herpertz-Dahlmann, K. Konrad, Meta-analytic evidence for a joint neural mechanism underlying response inhibition and state anger. Human brain mapping **41**(11), 3147–3160 (2020)

[61] J. Zhu, J. Li, X. Li, J. Rao, Y. Hao, Z. Ding, G. Wang, Neural basis of the emotional conflict processing in major depression: Erps and source localization analysis on the n450 and p300 components. Frontiers in human neuroscience **12**, 214 (2018)

[62] B. Zrenner, C. Zrenner, P.C. Gordon, P. Belardinelli, E.J. McDermott, S.R. Soekadar, A.J. Fallgatter, U. Ziemann, F. Müller-Dahlhaus, Brain oscillation-synchronized stimulation of the left dorsolateral prefrontal cortex in depression using real-time eeg-triggered tms. Brain stimulation **13**(1), 197–205 (2020)

[63] C. Zrenner, P. Belardinelli, F. Müller-Dahlhaus, U. Ziemann, Closed-loop neuroscience and non-invasive brain stimulation: a tale of two loops. Frontiers in cellular neuroscience **10**, 92 (2016)

[64] D. Schunk, E.M. Berger, H. Hermes, K. Winkel, E. Fehr, Teaching self-regulation. Nature Human Behaviour **6**(12), 1680–1690 (2022)

[65] D.V. Sheehan, Y. Lecrubier, K.H. Sheehan, P. Amorim, J. Janavs, E. Weiller, T. Hergueta, R. Baker, G.C. Dunbar, et al., The mini-international neuropsychiatric interview (mini): the development and validation of a structured diagnostic psychiatric interview for dsm-iv and icd-10. Journal of clinical psychiatry **59**(20), 22–33 (1998)

[66] R.C. Oldfield, The assessment and analysis of handedness: the edinburgh inventory. Neuropsychologia **9**(1), 97–113 (1971)

[67] T. Canli, M. Qiu, K. Omura, E. Congdon, B.W. Haas, Z. Amin, M.J. Herrmann, R.T. Constable, K.P. Lesch, Neural correlates of epigenesis. Proceedings of the National Academy of Sciences **103**(43), 16,033–16,038 (2006)

[68] J.H. Patton, M.S. Stanford, E.S. Barratt, Factor structure of the barratt impulsiveness scale. Journal of clinical psychology **51**(6), 768–774 (1995)

[69] W. Horn, Leistungsprüfsystem, lps: Handanweisung für die durchführung, auswertung und interpretation. (1962)

[70] B.A. Eriksen, C.W. Eriksen, Effects of noise letters upon the identification of a target letter in a nonsearch task. Perception & psychophysics **16**(1), 143–149 (1974)

[71] P.J. Lang, M.M. Bradley, B.N. Cuthbert, et al., International affective picture system (iaps): Technical manual and affective ratings. NIMH Center for the Study of Emotion and Attention **1**(39-58), 3 (1997)

[72] R.D. Luce, et al., *Response times: Their role in inferring elementary mental organization*. 8 (Oxford University Press on Demand, 1986)

[73] A.S. Hervey, J.N. Epstein, J.F. Curry, S. Tonev, L. Eugene Arnold, C. Keith Conners, S.P. Hinshaw, J.M. Swanson, L. Hechtman, Reaction time distribution analysis of neuropsychological performance in an adhd sample. Child Neuropsychology **12**(2), 125–140 (2006)

[74] O. Papaspiliopoulos, G.O. Roberts, M. Sköld, A general framework for the parametrization of hierarchical models. Statistical Science pp. 59–73 (2007)

[75] M. Betancourt, M. Girolami, Hamiltonian monte carlo for hierarchical models. Current trends in Bayesian methodology with applications **79**(30), 2–4 (2015)

[76] D. Bates, M. Mächler, B. Bolker, S. Walker, Fitting linear mixed-effects models using lme4. Journal of Statistical Software **67**(1), 1–48 (2015). https://doi.org/10.18637/jss.v067.i01

[77] M. Windhoff, A. Opitz, A. Thielscher, Electric field calculations in brain stimulation based on finite elements: an optimized processing pipeline for the generation and usage of accurate individual head models. Tech. rep., Wiley Online Library (2013)

[78] J. Vorwerk, R. Oostenveld, M.C. Piastra, L. Magyari, C.H. Wolters, The fieldtrip-simbio pipeline for eeg forward solutions. Biomedical engineering online **17**(1), 1–17 (2018)

[79] G.B. Saturnino, K.H. Madsen, A. Thielscher, Electric field simulations for transcranial brain stimulation using fem: an efficient implementation and error analysis. Journal of neural engineering **16**(6), 066,032 (2019)

[80] A.M. Dale, B. Fischl, M.I. Sereno, Cortical surface-based analysis: I. segmentation and surface reconstruction. Neuroimage **9**(2), 179–194 (1999)

[81] B. Fischl, M.I. Sereno, A.M. Dale, Cortical surface-based analysis: Ii: inflation, flattening, and a surface-based coordinate system. Neuroimage **9**(2), 195–207 (1999)

[82] S.M. Smith, Fast robust automated brain extraction. Human brain mapping **17**(3), 143–155 (2002)

[83] S. Gabriel, R. Lau, C. Gabriel, The dielectric properties of biological tissues: Ii. measurements in the frequency range 10 hz to 20 ghz. Physics in medicine & biology **41**(11), 2251 (1996)

[84] G. Birot, L. Spinelli, S. Vulliémoz, P. Mégevand, D. Brunet, M. Seeck, C.M. Michel, Head model and electrical source imaging: a study of 38 epileptic patients. NeuroImage: Clinical **5**, 77–83 (2014)

[85] R. Oostenveld, P. Fries, E. Maris, J.M. Schoffelen, Fieldtrip: open source software for advanced analysis of meg, eeg, and invasive electrophysiological data. Computational intelligence and neuroscience **2011** (2011)

[86] T.J. Sejnowski, in *Advances in Neural Information Processing Systems 8: Proceedings of the 1995 Conference*, vol. 8 (MIT press, 1996), p. 145

[87] M. Chaumon, D.V. Bishop, N.A. Busch, A practical guide to the selection of independent components of the electroencephalogram for artifact correction. Journal of neuroscience methods **250**, 47–63 (2015)

[88] B.V. Ehinger, P. König, J.P. Ossandón, Predictions of visual content across eye movements and their modulation by inferred information. Journal of Neuroscience **35**(19), 7403–7413 (2015)

[89] N. Kriegeskorte, W.K. Simmons, P.S. Bellgowan, C.I. Baker, Circular analysis in systems neuroscience: the dangers of double dipping. Nature neuroscience **12**(5), 535–540 (2009)

[90] E. Maris, R. Oostenveld, Nonparametric statistical testing of eeg-and meg-data. Journal of neuroscience methods **164**(1), 177–190 (2007)

[91] D. Jeffreys, J. Axford, Source locations of pattern-specific components of human visual evoked potentials. i. component of striate cortical origin. Experimental brain research **16**(1), 1–21 (1972)

[92] F. Di Russo, A. Martínez, M.I. Sereno, S. Pitzalis, S.A. Hillyard, Cortical sources of the early components of the visual evoked potential. Human brain mapping **15**(2), 95–111 (2002)

[93] J. Gross, J. Kujala, M. Hämäläinen, L. Timmermann, A. Schnitzler, R. Salmelin, Dynamic imaging of coherent sources: studying neural interactions in the human brain. Proceedings of the National Academy of Sciences **98**(2), 694–699 (2001)

[94] D.B. Percival, A.T. Walden, et al., *Spectral analysis for physical applications* (cambridge university press, 1993)

[95] M.J. Brookes, J. Vrba, S.E. Robinson, C.M. Stevenson, A.M. Peters, G.R. Barnes, A. Hillebrand, P.G. Morris, Optimising experimental design for meg beamformer imaging. Neuroimage **39**(4), 1788–1802 (2008)

[96] M.X. Huang, J. Shih, R. Lee, D. Harrington, R. Thoma, M. Weisend, F. Hanlon, K. Paulson, T. Li, K. Martin, et al., Commonalities and differences among vectorized beamformers in electromagnetic source imaging. Brain topography **16**(3), 139–158 (2004)

[97] S. Helbling, Advances in meg methods and their applications to investigate auditory perception. doctoralthesis, Universitätsbibliothek Johann Christian Senckenberg (2017)

[98] J. Gross, S. Baillet, G.R. Barnes, R.N. Henson, A. Hillebrand, O. Jensen, K. Jerbi, V. Litvak, B. Maess, R. Oostenveld, et al., Good practice for conducting and reporting meg research. Neuroimage **65**, 349–363 (2013)

[99] J.R. King, S. Dehaene, Characterizing the dynamics of mental representations: the temporal generalization method. Trends in cognitive sciences **18**(4), 203–210 (2014)

[100] M.N. Hebart, C.I. Baker, Deconstructing multivariate decoding for the study of brain function. Neuroimage **180**, 4–18 (2018)

[101] M. Guggenmos, P. Sterzer, R.M. Cichy, Multivariate pattern analysis for meg: A comparison of dissimilarity measures. NeuroImage **173**, 434–447 (2018)

[102] C.C. Chang, C.J. Lin, Libsvm: a library for support vector machines. ACM transactions on intelligent systems and technology (TIST) **2**(3), 1–27 (2011)

[103] JASP Team. JASP (Version 0.16)[Computer software] (2021). URL https://jasp-stats.org/

[104] M. Dhamala, G. Rangarajan, M. Ding, Analyzing information flow in brain networks with nonparametric granger causality. Neuroimage **41**(2), 354–362 (2008)

[105] X. Wang, Y. Chen, S.L. Bressler, M. Ding, Granger causality between multiple interdependent neurobiological time series: blockwise versus pairwise methods. International journal of neural systems **17**(02), 71–78 (2007)

[106] J. Salvatier, T.V. Wiecki, C. Fonnesbeck, Probabilistic programming in python using PyMC3. PeerJ Computer Science **2**, e55 (2016). https://

doi.org/10.7717/peerj-cs.55. URL https://doi.org/10.7717/peerj-cs.55

[107] G. Van Rossum, F.L. Drake, *Python 3 Reference Manual* (CreateSpace, Scotts Valley, CA, 2009)

[108] Anaconda software distribution (2020). URL https://docs.anaconda.com/

[109] D.J. Barr, Random effects structure for testing interactions in linear mixed-effects models. Frontiers in psychology **4**, 328 (2013)

[110] R Core Team, *R: A Language and Environment for Statistical Computing*. R Foundation for Statistical Computing, Vienna, Austria (2018). URL https://www.R-project.org/

[111] D. Bates, D. Sarkar, M.D. Bates, L. Matrix, The lme4 package. R package version **2**(1), 74 (2007)

Acknowledgments. This project was funded by German Research Foundation (CRC 1193, project C04, MW and OT). MW, Volkswagen Stiftung, Award ID: Big Data in den Lebenswissenschaften. MW, Niedersächsisches Ministerium für Wissenschaft und Kultur (https://dx.doi.org/10.13039/501100010570), Award ID: Niedersächsisches Vorab. We thank Shirin Hagner, Kristin Weineck, Sarah Brosche and Svenja Hummel for their help in data collection.

Appendix A Supplementary Material

A.1 Supplementary information about behavioral effects of emotion-cognition interaction

The average reaction time was $547.75 \pm 51.74ms$. The increased cognitive load during incongruent versus congruent trials slowed down the reaction time by 95.2 ms on average. The increased emotional interference during negative compared to neutral trials slowed down the reaction time by 8.2 ms on average. The mean reaction time were $601.6 \pm 59.49ms$ for negative incongruent trials, $593.6 \pm 58.96ms$ for neutral incongruent trials, $506.6 \pm 44.55ms$ for negative congruent trials and $498.2 \pm 43.97ms$ for neutral congruent trials. There was a stronger emotional interference when the cognitive load was lower, as the difference on incongruent minus congruent for negative was 90.4 ms compared to 95.4 ms for neutral trials. This means subjects are slowed down in their reaction time due to higher emotional valence (negative) especially when the cognitive load is lower (congruent Flanker). For reaction time, a linear mixed effect model was used to predict reaction time based on an interaction of emotion (i.e., negative/neutral) and cognition (incongruent/congruent) as main effects, allowing for different intercepts per subject (random effects). For accuracy, the same model was used in a general linear mixed effect model approach.

Both models were statistically tested against the respective null model, the same model but without the interaction term. To test for statistical significance of the interaction term, a maximum likelihood ratio approach [109] was used to compare the models. Model coding was done in R [110] with the lmer and glmer function from the lme4-package [111]. To test whether modeling the interaction is more informative compared to the null model without the interaction when predicting the reaction time, a maximum likelihood ratio was computed. The interaction of emotional load and cognitive load is significant (p=0.001563) in terms of reaction time (see supplementary Table A1). The accuracy was generally high, as the average accuracy was $95.18 \pm 4.79\%$ suggesting an easy feasibility of the task. Nevertheless, the increased cognitive load of incongruent compared to congruent trials led to a drop in accuracy of 7.15 % on average. The increased emotional interference during negative compared to neutral trials led to a drop in accuracy of 0.55 % on average. The mean accuracy was $91.2 \pm 7.14\%$ for negative incongruent, $92.0 \pm 7.38\%$ for neutral incongruent, $98.6 \pm 2.53\%$ for negative congruent and $98.9 \pm 2.1\%$ for neutral congruent trials. There was a stronger emotional interference when the cognitive load was higher, as the difference on incongruent minus congruent for negative was -7.4% compared to -6.8% for neutral. This means subjects make more incorrect responses during high cognitive load (incongruent Flanker) especially with high emotional load (negative valence). In sum, the cognitive effect was ten times stronger than the emotional effect, which in turn was ten times stronger than the interaction effect on the level of behavior (see Fig. 1). To test whether modeling the interaction is more informative compared to the null model without the interaction when predicting the accuracy, a maximum likelihood ratio was computed. The interaction of emotional load and cognitive load is not significant (p=0.2199) in terms of accuracy (see Table A1).

Table A1 Results for the frequentist linear mixed models for reaction times and accuracy

Model	AIC	BIC	deviance	χ^2	χ df	p
RT Null Model	-350810	-350761	-350820	NA	NA	NA
RT Interaction Model	-350818	-350759	-350830	10.002	1	0.001563**
Acc Null Model	41713	41752	41705	NA	NA	NA
Acc Interaction Model	41714	41762	41704	1.5052	1	0.2199

A.2 Supplementary Results of EEG source reconstruction

A.2.1 Definition of frequency bands of interest at the sensor level

To identify frequency bands of interest for the subsequent source-level analysis, we computed the contrast task against baseline at the sensor level, and identified four frequency bands of interest: θ 7 ± 2 Hz, β 21 ± 12 Hz, γ 49 ± 16 Hz

Table A2 Priors of Hierarchical Bayesian linear regression for reaction time and accuracy

parameter	value
$\alpha_{intercept}$	$Normal\ (\mu = 0, \sigma = 5)$
β_E	$Normal(\mu = 0, \sigma = 3)$
β_C	$Normal(\mu = 0, \sigma = 3)$
β_{EC}	$Normal(\mu = 0, \sigma = 3)$
α_{offset}	$Normal(\mu = 0, \sigma = 1)$
β_{E_offset}	$Normal(\mu = 0, \sigma = 1)$
β_{C_offset}	$Normal(\mu = 0, \sigma = 1)$
σ	$HalfNormal\ (\sigma = 1)$

Table A3 Mean reaction time and mean accuracy per subject was predicted based on E, C and EC contrast (see Referencessubsection:bayesianbehavior)

and high γ 102 $\pm$ 38 Hz (center frequency $\pm$ spectral smoothing) for both time windows of interest before (tROI Emo) and after (tROI Flanker) (Fig. A1).

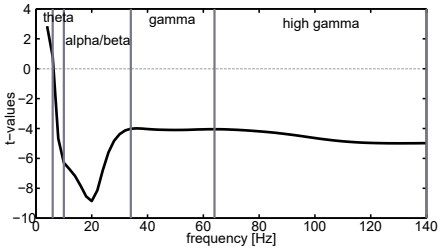

Fig. A1 Spectral sensor level analysis for the task-independent definition of frequency bands of interest. Power spectrum analysis, obtained from pooled task conditions versus baseline to determine frequency bands (n=103). Grey lines in the power spectrum frame the frequency ranges of interest for subsequent beamforming analysis

A.2.2 Supplementary results of source localization

In order to identify neural sources significantly modulated by the factors emotion and cognition in our task, and by their interaction, we reconstructed sources of each contrast (E, C and EC), both, before (tROI Emo) and after (tROI Flanker) Flanker signal onset. In Tab. A4 we report the full results of four different frequency bands, θ 7 $\pm$ 2 Hz, β 21 $\pm$ 12 Hz, γ 49 $\pm$ 16 Hz and high γ 102 $\pm$ 38 Hz (center frequency $\pm$ spectral smoothing) for both time windows of interest – before (tROI Emo) and after (tROI Flanker).

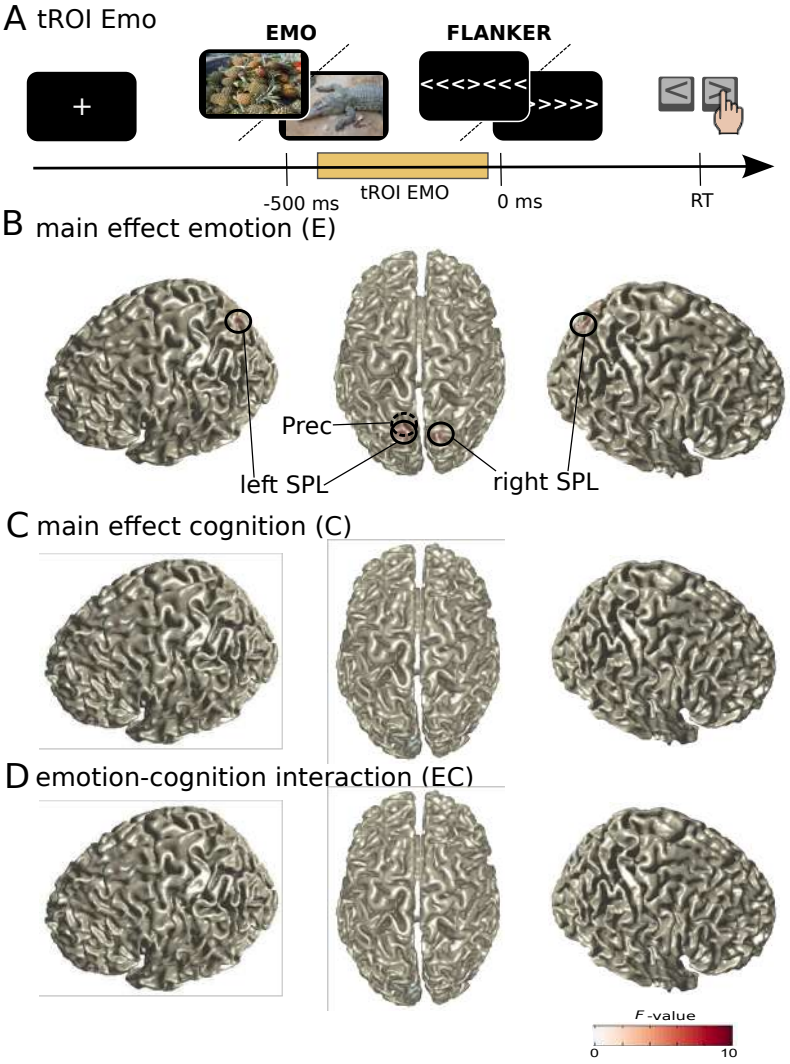

Fig. A2 Source activity in the θ band (5-9 Hz) during tROI Emo. Surface plots show significant F-values of ANOVA (cluster-based permutation test, Bonferroni corrected for four frequency bands and two time windows, alpha and clusteralpha <0.00625, n=103). Peak voxels (local extrema) of significant clusters are indicated with circles and labels (for MNI coordinates, see Tab. A4). Dashed circles mark peak voxels invisible in this representation. A, Task design and analyzed tROI; B, main effect of emotion (E); C, main effect of cognition (C); D, interaction effect between emotion and cognition (EC).

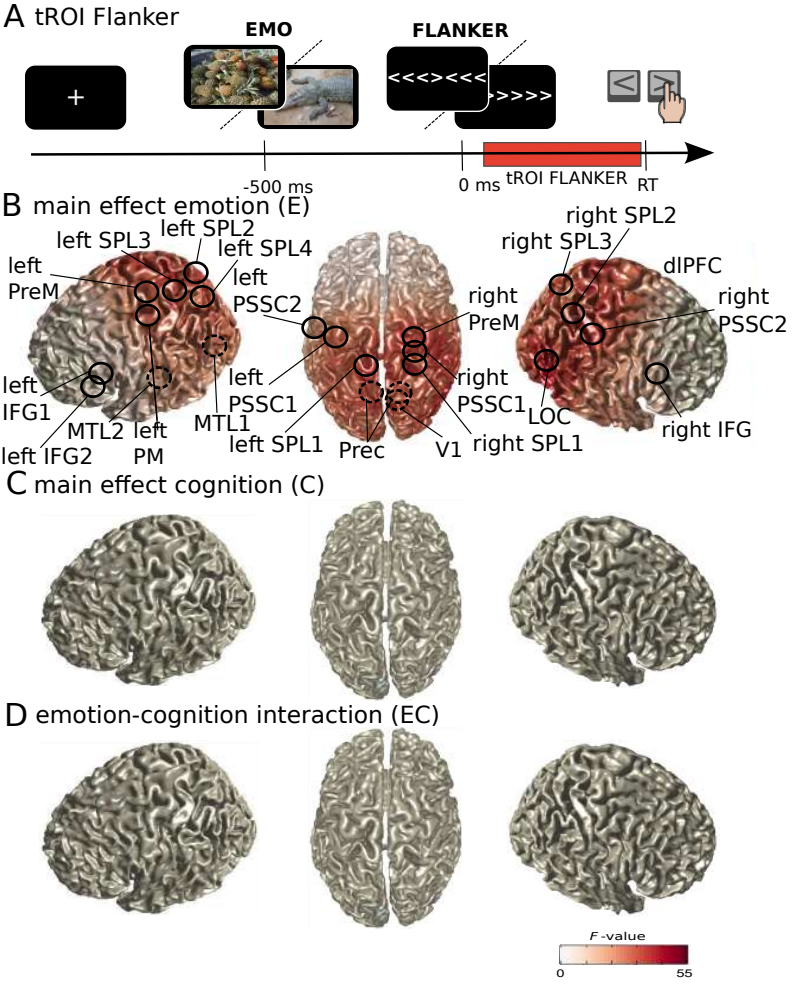

Fig. A3 Source activity in the θ band (5-9 Hz) during tROI Flanker. Surface plots show significant F-values of ANOVA (cluster-based permutation test, Bonferroni corrected for four frequency bands and two time windows, alpha and clusteralpha <0.00625, n=103). Peak voxels (local extrema) of significant clusters are indicated with circles and labels (for MNI coordinates, see Tab. A4). Dashed circles mark peak voxels invisible in this representation. A, Task design and analyzed tROI; B, main effect of emotion (E); C, main effect of cognition (C); D, interaction effect between emotion and cognition (EC).

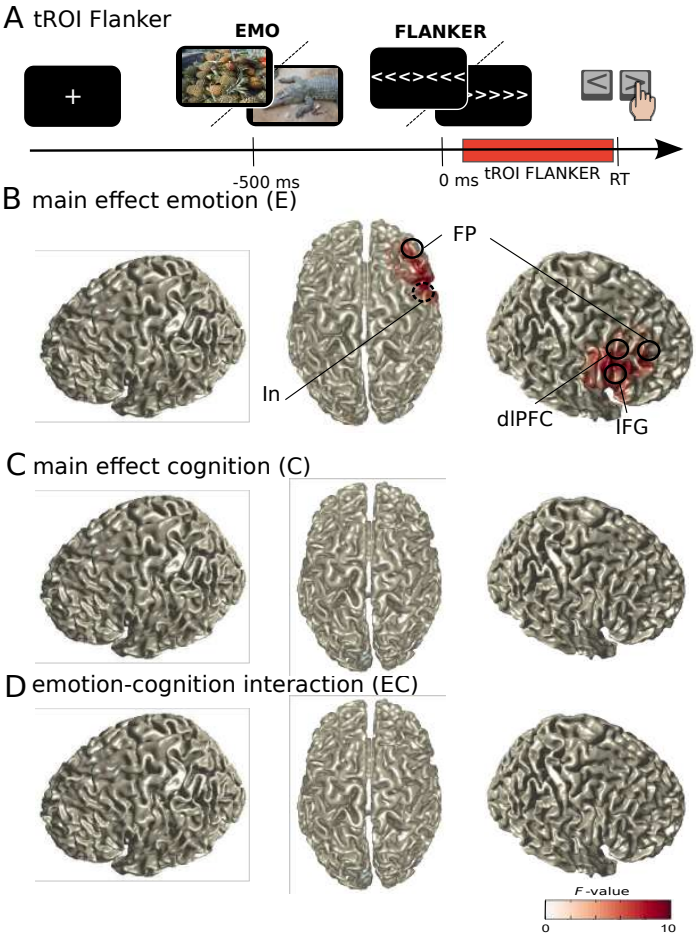

Fig. A4 Source activity in the γ band (33-65 Hz) during tROI Flanker. Surface plots show significant F-values of ANOVA (cluster-based permutation test, Bonferroni corrected for four frequency bands and two time windows, alpha and clusteralpha <0.00625, n=103). Peak voxels (local extrema) of significant clusters are indicated with circles and labels (for MNI coordinates, see Tab. A4). Dashed circles mark peak voxels invisible in this representation. A, Task design and analyzed tROI; B, main effect of emotion (E); C, main effect of cognition (C); D, interaction effect between emotion and cognition (EC).

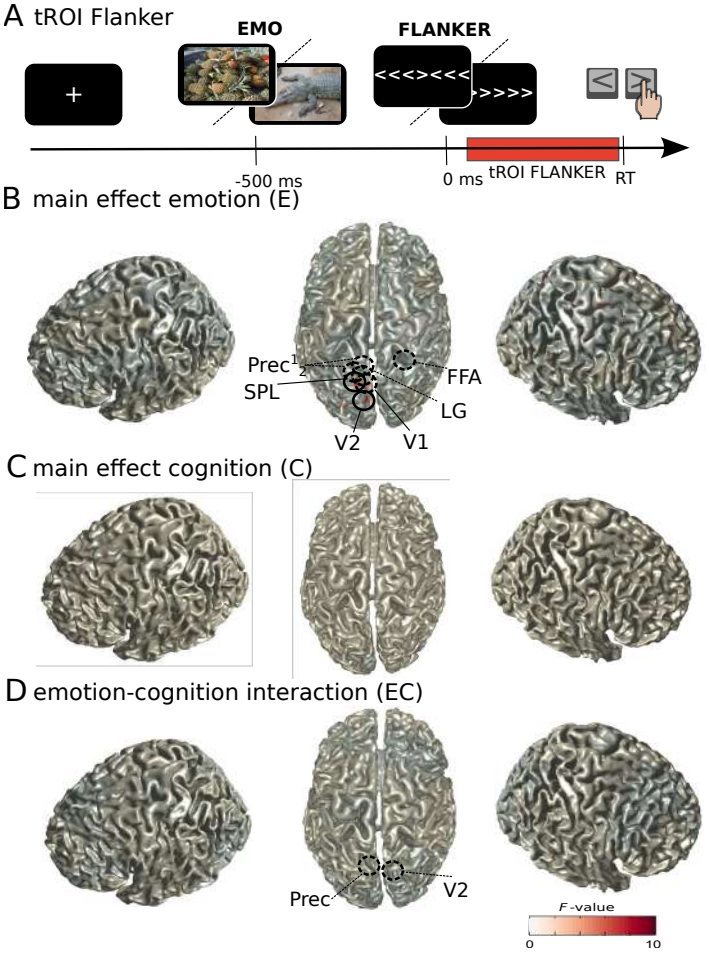

Fig. A5 Source activity in the High γ band (64-140 Hz) during tROI Flanker. Surface plots show significant F-values of ANOVA (cluster-based permutation test, Bonferroni corrected for four frequency bands and two time windows, alpha and clusteralpha <0.00625, n=103). Peak voxels (local extrema) of significant clusters are indicated with circles and labels (for MNI coordinates, see Tab. A4). Dashed circles mark peak voxels invisible in this representation. A, Task design and analyzed tROI; B, main effect of emotion (E); C, main effect of cognition (C); D, interaction effect between emotion and cognition (EC).

A.2.3 Supplementary information on Bayesian priors

Freq.	tROI.	Contr.	Region (label)	Coordinat. (x,y,z)	Source F-value	p.e. (Mean)	Bootstrap 95% CI	Cluster F-value	Cluster P-value
θ	EMO	E	Superior Parietal Lobe (rSPL) R	15 -80 60	11.1455	-0.4158	[-0.6641; -0.1692]	11.1455	3.9992e-04
θ	EMO	E	Precuneus (lPrec) L	-5 -70 40	8.9030	-0.3417	[-0.5697; -0.1146]	33.0149	1.9996e-04
θ	EMO	E	Superior Parietal Lobe (lSPL) L	-25 -90 50	8.3064	-0.3503	[-0.5858; -0.1043]	8.3064	3.9992e-04
θ	Flanker	E	Lateral Occipital Cortex (rLOC) R	55 -70 10	46.6805	-0.8177	[-1.0558; -0.5825]	6.1468e+04	1.9996e-04
θ	Flanker	E	Superior Parietal Lobe (rSPL) R	25 -50 40	44.4014	-0.7868	[-1.0194; -0.5505]	6.1468e+04	1.9996e-04
θ	Flanker	E	Primary Visual Cortex (rV1) R	5 -80 10	43.9917	-0.7519	[-0.9778; -0.5291]	6.1468e+04	1.9996e-04
θ	Flanker	E	Primary Somatosensory Cortex R (rPSSC), BA2	25 -40 60	43.9502	-0.7575	[-0.9854; -0.5344]	6.1468e+04	1.9996e-04
θ	Flanker	E	Superior Parietal Lobe L (lSPL)	-15 -40 80	41.8829	-0.7834	[-1.0158; -0.5373]	6.1468e+04	1.9996e-04
θ	Flanker	E	Precuneous Cortex R (rPrec)	15 -70 30	41.7265	-0.7527	[-0.9829; -0.5226]	6.1468e+04	1.9996e-04
θ	Flanker	E	Primary Somatosensory Cortex R (rPSSC), BA1	55 -20 60	41.3273	-0.6751	[-0.8769; -0.4609]	6.1468e+04	1.9996e-04
θ	Flanker	E	Premotor Cortex R (rPM)	25 -20 80	41.1597	-0.6969	[-0.9070; -0.4762]	6.1468e+04	1.9996e-04
θ	Flanker	E	Precuneous Cortex L (lPrec)	-5 -70 30	41.0866	-0.7976	[-1.0435; -0.5524]	6.1468e+04	1.9996e-04
θ	Flanker	E	Superior Parietal Lobe L (lSPL)	-5 -80 60	40.6483	-0.7424	[-0.9750; -0.5121]	6.1468e+04	1.9996e-04
θ	Flanker	E	Inferior Parietal Lobe R (rIPL)	55 -40 40	40.2498	-0.7208	[-0.9448; -0.4948]	6.1468e+04	1.9996e-04
θ	Flanker	E	Superior Parietal Lobe (rSPL) R	15 -80 60	40.0227	-0.7825	[-1.0306; -0.5403]	6.1468e+04	1.9996e-04
θ	Flanker	E	Superior Parietal Lobe L (lSPL)	-15 -50 60	38.5924	-0.7574	[-0.9965; -0.5163]	6.1468e+04	1.9996e-04
θ	Flanker	E	Superior Parietal Lobe L (lSPL)	-25 -80 60	38.1349	-0.7820	[-1.0372; -0.5379]	6.1468e+04	1.9996e-04
θ	Flanker	E	Cerebellum R (rCer)	15 -50 -30	37.2761	-0.7205	[-0.9513; -0.4818]	6.1468e+04	1.9996e-04
θ	Flanker	E	Cerebellum R (rCer)	5 -80 -30	35.5559	-0.7370	[-0.9811; -0.4893]	6.1468e+04	1.9996e-04
θ	Flanker	E	Primary Somatosensory Cortex L (lPSSC)	-55 -20 60	34.9523	-0.6195	[-0.8256; -0.4114]	6.1468e+04	1.9996e-04
θ	Flanker	E	Primary Motor Cortex L (lPrM)	-35 -10 70	33.6669	-0.6428	[-0.8573; -0.4141]	6.1468e+04	1.9996e-04
θ	Flanker	E	Premotor Cortex L (lPM)	-15 -10 80	33.4476	-0.6700	[-0.8955; -0.4347]	6.1468e+04	1.9996e-04
θ	Flanker	E	Primary Somatosensory Cortex L (lPSSC)	-65 -10 40	28.6332	-0.5728	[-0.7849; -0.3628]	6.1468e+04	1.9996e-04
θ	Flanker	E	Middle Temporal Lobe L (lTL)	-65 -60 10	26.4450	-0.6204	[-0.8632; -0.3853]	6.1468e+04	1.9996e-04
θ	Flanker	E	Middle Temporal Lobe L (lTL)	-65 0 -10	18.5366	-0.4800	[-0.7096; -0.2655]	6.1468e+04	1.9996e-04
θ	Flanker	E	Inferior Frontal Gyrus R (rIFG)	55 40 0	15.3509	-0.4218	[-0.6327; -0.2090]	6.1468e+04	1.9996e-04
θ	Flanker	E	Inferior Frontal Gyrus L (lIFG)	-55 40 10	12.1197	-0.3917	[-0.6177; -0.1716]	6.1468e+04	1.9996e-04
θ	Flanker	E	Inferior Frontal Gyrus L (lIFG)	-45 50 20	11.2494	-0.3972	[-0.6322; -0.1639]	11.2494	1.9996e-04
β	Flanker	E	Fusiform Face Area R (rFFA)	35 -50 10	16.1438	0.4319	[0.2187; 0.6455]	5.2295e+0.3	<1.9996e-04
β	Flanker	E	dorsomedial Prefrontal Cortex R (rdmPFC)	5 40 40	15.9367	0.4302	[0.2212; 0.6483]	5.2295e+0.3	<1.9996e-04
β	Flanker	E	dorsolateral Prefrontal Cortex R (rdlPFC)	25 30 60	13.5796	0.3963	[0.1808; 0.6073]	5.2295e+0.3	<1.9996e-04
β	Flanker	E	lateral Occipital Cortex R (rLOC)	35 -70 30	13.3564	0.3686	[0.1680; 0.5689]	5.2295e+0.3	<1.9996e-04
β	Flanker	E	Frontal Pole R (rFP)	5 60 40	12.8408	0.4005	[0.1744; 0.6177]	5.2295e+0.3	<1.9996e-04
β	Flanker	E	Angular Gyrus R (rAG)	45 -50 20	12.6571	0.3737	[0.1714; 0.5859]	5.2295e+0.3	<1.9996e-04
β	Flanker	E	Superior Frontal Gyrus R (rSFG)	25 10 60	12.4352	0.3686	[0.1613; 0.5781]	5.2295e+0.3	<1.9996e-04
β	Flanker	E	Premotor Cortex R (rPM)	45 0 50	11.2470	0.3553	[0.1453; 0.5647]	19.5099	<1.9996e-04
β	Flanker	E	Inferior Frontal Gyrus R (rIFG)	45 40 0	10.4409	0.3852	[0.1510; 0.6221]	5.2295e+0.3	<1.9996e-04
β	Flanker	E	Precuneous Cortex R (rPrec)	15 -70 50	9.7742	0.3459	[0.1311; 0.5695]	5.2295e+0.3	<1.9996e-04
β	Flanker	E	Frontal Pole L (lFP)	-25 50 10	9.6548	0.3641	[0.1238; 0.5947]	25.9950	<1.9996e-04
β	Flanker	E	Primary Somatosensory Cortex R (rPSSC)	45 -10 30	8.8410	0.3268	[0.1172; 0.5519]	5.2295e+0.3	<1.9996e-04
β	Flanker	E	Inferior Frontal Gyrus L (lIFG)	-35 30 10	8.7014	0.3131	[0.1040; 0.5265]	8.7014	<1.9996e-04
β	Flanker	E	Primary Motor Cortex R (rPrMC)	35 -20 50	8.2433	0.3131	[0.1016; 0.5327]	8.2433	<1.9996e-04
β	Flanker	C	dorsolateral Prefrontal Cortex R (rdlPFC)	45 20 30	8.5053	0.3048	[0.1082; 0.5220]	8.5053	<1.9996e-04
β	Flanker	C	medial Temporal Lobe R (rmTL)	65 -10 -10	8.3118	0.3278	[0.1194; 0.5716]	8.3118	<1.9996e-04
β	Flanker	C	Inferior Frontal Gyrus R (rIFG)	55 10 10	7.9618	0.3034	[0.1010; 0.5278]	7.9618	<1.9996e-04
β	Flanker	EC	Inferior Frontal Gyrus R (rIFG)	45 40 20	9.6267	-0.5948	[-0.9589;-0.1966]	9.6267	<1.9996e-04
γ	Flanker	E	dorsolateral Prefrontal Cortex R (dlPFC)	55 20 40	14.7569	0.3379	[0.1642; 0.5134]	586.3702	<1.9996e-04
γ	Flanker	E	Inferior Frontal Gyrus R (IFG)	65 20 10	14.1434	0.3717	[0.1730; 0.5644]	586.3702	<1.9996e-04
γ	Flanker	E	orbitofrontal Frontal Pole R (oFP)	35 50 30	12.9234	0.2990	[0.1364; 0.4642]	586.3702	<1.9996e-04
γ	Flanker	E	Insula R (In)	45 20 -10	12.7424	0.3383	[0.1470;0.5234]	586.3702	<1.9996e-04
γ	Flanker	E	ventromedial Frontal Pole R (vFP)	15 60 0	9.2366	0.2885	[0.1052; 0.4790]	9.2366	0.0028
High γ	Flanker	E	Superior Parietal Lobe L (lSPL)	-15 -70 60	10.5863	-0.2977	[-0.4814; -0.1177]	10.5863	<1.9996e-04
High γ	Flanker	E	Secondary Visual Cortex L (lV2)	-5 -80 30	9.6571	-0.2956	[-0.4866; -0.1086]	17.8269	<1.9996e-04
High γ	Flanker	E	Primary Visual Cortex V1 L (lV1)	-5 -80 10	8.9396	-0.3073	[-0.5139; -0.1080]	8.9396	<1.9996e-04
High γ	Flanker	E	Lingual Gyrus L (lLG)	-5 -70 -10	8.4952	-0.2811	[-0.4740; -0.0921]	8.4952	<1.9996e-04
High γ	Flanker	E	Fusiform Face Area R (rFFA)	25 -50 10	8.4180	-0.2715	[-0.4545; -0.0857]	8.4180	<1.9996e-04
High γ	Flanker	E	Precuneous Cortex L 1 (lPrec)	-5 -60 10	8.3565	-0.2789	[-0.4714; -0.0882]	8.3565	<1.9996e-04
High γ	Flanker	E	Precuneous Cortex L 2 (lPrec)	-5 -60 30	8.3055	-0.2913	[-0.4961; -0.0943]	8.3055	<1.9996e-04
High γ	Flanker	EC	Secondary Visual Cortex R (rV2)	5 -80 20	7.9948	-0.4994	[-0.8461; -0.1485]	7.9948	<1.9996e-04
High γ	Flanker	EC	Precuneous Cortex L (lPrec)	-5 -60 30	7.8551	-0.4667	[-0.7983; -0.1334]	7.8551	<1.9996e-04

Table A4 Overview of significant sources. Significant sources for all frequency bands and tROIs are given for the contrasts (Contr.) of emotion (E), cognition (C) and emotion-cognition interaction (EC). The table shows sources (Region (label)) with respective coordinates and F-values. Furthermore, it shows the point estimate (p.e.) of source activity (mean difference for main effects mean double difference for interaction effects) and the bootstrap Confidence-Interval of the effect (95% CI). Additional Cluster F- and P-values are presented.

Table A5 Priors of Bayesian linear regression between reaction time, accuracy, and min/max β-band interaction values

parameter	value
ρ	*Uniform* $(a = -1, b = 1)$

Table A6 Mean reaction time and mean accuracy per subject was predicted based on min/max β-band interaction values (see Bayesian correlation of min/max β power interaction values with behavioral measures and Fig. 1).

Table A7 Priors of Bayesian linear regression between reaction time, accuracy, and min/max β power

parameter	value
$\alpha_{intercept}$	$Normal\ (\mu = 0, \sigma = 1)$
$\beta_{mean_{power}}$	$Normal(\mu = 0, \sigma = 1)$
β_E	$Normal(\mu = 0, \sigma = 1)$
β_C	$Normal(\mu = 0, \sigma = 1)$
β_{EC}	$Normal(\mu = 0, \sigma = 1)$
σ	$HalfNormal\ (\sigma = 1)$

Table A8 Mean reaction time and mean accuracy per subject was predicted based on the average, E, C and EC min/max β-band values (see Bayesian linear regression of β power with behavioral measures and Fig. 5).

Table A9 Priors of Bayesian linear regression between reaction time, accuracy and cGC

parameter	value
$\alpha_{intercept}$	$Normal\ (\mu = 0, \sigma = 0.5)$
β_{links}	$Normal(\mu = 0, \sigma = 0.5)$
$\beta_{links^{\Delta}}$	$Normal(\mu = 0, \sigma = 0.5)$
σ	$HalfNormal\ (\sigma = 1)$

Table A10 Mean reaction time and mean accuracy per subject were predicted based on cGC of each significant link of respective significant frequencies in the respective significant E, C, EC contrast (see Correlation of top-down Granger Causality with behavior and Fig.8).